

# NGC 346 IN THE SMALL MAGELLANIC CLOUD. III. RECENT STAR FORMATION AND STELLAR CLUSTERING PROPERTIES IN THE BRIGHT HII REGION N 66<sup>1</sup>

EVA HENNEKEMPER, DIMITRIOS A. GOULIERMIS, THOMAS HENNING, WOLFGANG BRANDNER  
 Max-Planck-Institute for Astronomy, Königstuhl 17, 69117 Heidelberg, Germany

AND

ANDREW E. DOLPHIN  
 Raytheon Corporation, USA

*Accepted for Publication in ApJ October 2, 2007*

## ABSTRACT

In the third part of our photometric study of the star-forming region NGC 346/N 66 and its surrounding field in the Small Magellanic Cloud (SMC), we focus on the large number of low-mass pre-main sequence (PMS) stars revealed by the Hubble Space Telescope Observations with the Advanced Camera for Surveys. We investigate the origin of the observed broadening of the pre-main sequence population in the  $V-I$ ,  $V$  CMD. The most likely explanations are either the presence of differential reddening or an age spread among the young stars. Assuming the latter, simulations indicate that we cannot exclude the possibility that stars in NGC 346 might have formed in two distinct events occurring about 10 and 5 Myr ago, respectively. We find that the PMS stars are not homogeneously distributed across NGC 346, but instead are grouped in at least five different clusters. On spatial scales from  $0.8''$  to  $8''$  (0.24 to 2.4 pc at the distance of the SMC) the clustering of the PMS stars as computed by a two-point angular correlation function is self-similar with a power law slope  $\gamma \approx -0.3$ . The clustering properties are quite similar to Milky Way star forming regions like Orion OB or  $\rho$  Oph. Thus molecular cloud fragmentation in the SMC seems to proceed on the same spatial scales as in the Milky Way. This is remarkable given the differences in metallicity and hence dust content between SMC and Milky Way star forming regions.

*Subject headings:* Magellanic Clouds — Color-Magnitude diagram — stars: evolution — galaxies: star clusters — clusters: individual (NGC 346)

## 1. INTRODUCTION

It is well known that Galactic OB associations also host large numbers of fainter, low-mass pre-main sequence (PMS) stars (e.g. Preibisch & Zinnecker 1999; Sherry et al. 2004; Briceño et al. 2005). Low-mass PMS stars in stellar associations provide a longer-lasting record of the most recent star formation events than the short-lived high-mass stars. Large-scale surveys have identified hundreds of PMS stars in nearby OB associations (Briceño et al. 2007). In order to understand the star formation triggering and history, or the Initial Mass Function (IMF), one has to study both high- and low-mass stars in star forming regions.

In many cases the low-mass populations of galactic OB associations cannot be easily distinguished from foreground main-sequence stars (e.g. Briceño et al. 2001). Recently PMS stars have been discovered for the first time in an extragalactic stellar association, which suffers much less from contamination by the galactic disk. *Hubble Space Telescope* (HST) observations of the association LH 52 in the Large Magellanic Cloud (LMC) revealed  $\approx 500$  PMS stars with masses down to  $0.3 M_{\odot}$  (Gouliermis et al. 2006a). The investigation of individual extragalactic pre-main sequence stars opens a new field of study. As both high angular resolution and wide field-of-view are required, HST is the ideal observatory to carry out these studies. While HST observations of extragalactic associations cannot reach the detection limits achieved for local associations, they provide a unique opportunity for studying low-mass star formation in other galaxies.

The OB association NGC 346 in the Small Magellanic

Cloud (SMC) is located in the central part of the brightest H II region in the SMC, named LHA 115-N 66 or in short N 66 (Henize 1956). With 33 spectroscopically confirmed O and B stars, NGC 346 hosts the largest sample of young, massive stars in the SMC (Walborn 1978; Walborn & Blades 1986; Niemela et al. 1986; Massey et al. 1989; Walborn et al. 2000; Evans et al. 2006). Photoionization models by Relaño et al. (2002) imply that these stars are a major source of ionizing flux for the surrounding diffuse interstellar medium (ISM). Recent imaging from the Wide-Field Channel (WFC) of the *Advanced Camera for Surveys* (ACS) on-board HST (GO Program 10248; PI: A. Nota) revealed the PMS stellar content of the general region of NGC 346/N 66 down to the sub-solar mass regime (Nota et al. 2006; Gouliermis et al. 2006b – hereafter Paper I –; Sabbi et al. 2007). Nota et al. (2006) suggest that all PMS stars in the association are the product of a single star formation event, taking place 3 to 5 Myr ago. The PMS distribution in the  $V-I$ ,  $V$  color-magnitude diagram (CMD), however, shows a prominent widening, which may be explained by an age spread of  $\approx 10$  Myr. This raises the question *if the PMS stars in NGC 346 are indeed the result of a single star formation event*.

Sabbi et al. suggest that the PMS population is mainly concentrated in a number of subclusters (three of them at the central part, where the association is located), which formed at the same time from the turbulence-driven density variations, and not following a sequential process. Star counts, however, reveal only a few compact PMS clusters with a significant number of stars in the area around the association. The main body of the association cannot be divided into separate subclusters (Paper I). *Could the remote clusters be the product of a star formation event occurring before or after the event*

<sup>1</sup> Research supported by the Deutsche Forschungsgemeinschaft (German Research Foundation)

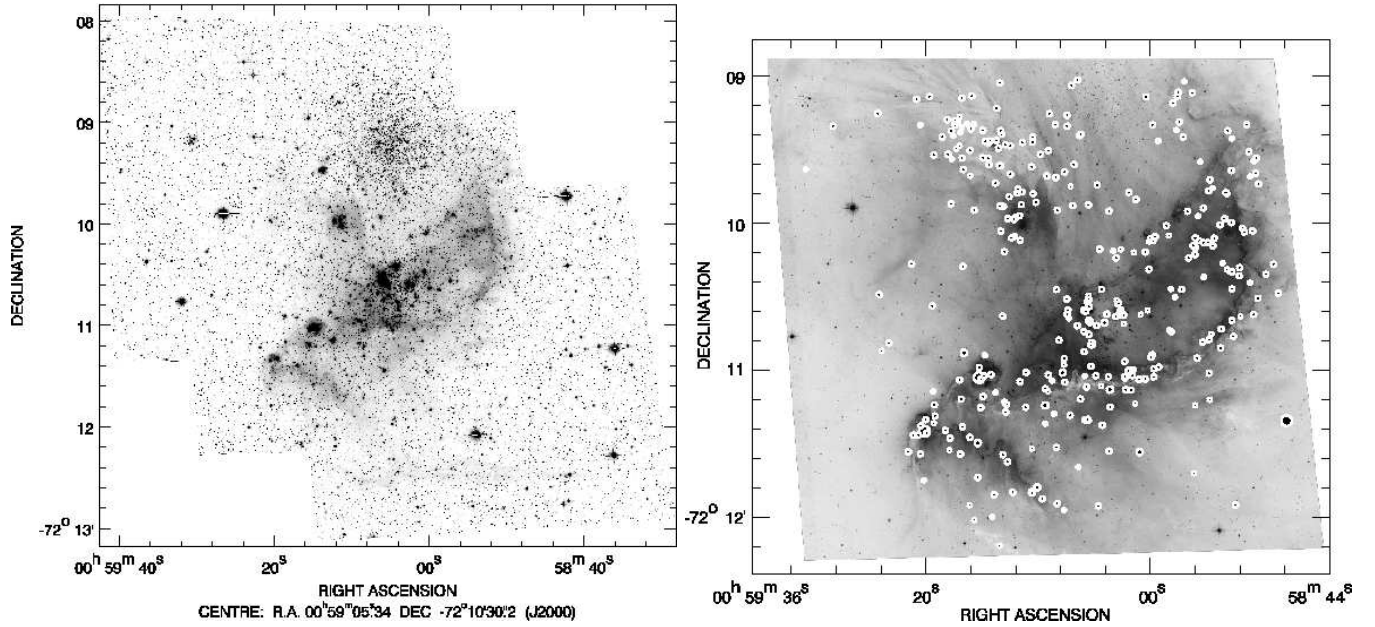


FIG. 1.— Left: ACS/WFC observations of NGC 346, composed of three overlapping pointings in the  $I$ -band. The association NGC 346 covers the center of the field, located almost in the middle of the “bar” of N 66, as it is outlined by the nebulosity. The intermediate-age cluster BS 90 (Rochau et al. 2007) is seen as the circular stellar concentration to the north of the association. Right: On the ACS/WFC  $H\alpha$  image of NGC 346/N 66 stars with intrinsic  $H\alpha$  excess are marked by circles. The spatial distribution of the excess stars outlines the HII region, and coincides with the overall distribution of the PMS stars.

which triggered the formation of the association?

In the first part of our study of this extraordinary star-forming region (Paper I), we compiled our ACS photometry of almost 100,000 stars, and presented preliminary results on stellar types and their distinct spatial distributions. We confirmed the co-existence of massive OB stars and low-mass PMS stars in NGC 346. In the present paper, we explore in greater detail the properties of the low-mass PMS stars with a focus on clustered star formation in NGC 346/N 66.

The paper is organized as follows: In § 2 we describe the datasets from HST/ACS, present the color-magnitude diagram, carry out a comparison of our photometry of the brightest stars with previous photometric studies, and discuss the reddening in the region. The broadening of the PMS distribution in the CMD, a thorough discussion of possible causes and explanations of this phenomenon as well as the spatial variations in the CMD are presented in § 3. In § 4 we present the clustering properties of the PMS stars and discuss them in terms of hierarchical star formation. Our analysis of  $H\alpha$  observations with HST/ACS as well as previous *Spitzer* Space Telescope results on Young Stellar Objects (YSOs) are presented in § 5 and § 6, respectively. In § 7 we summarize the results.

## 2. DESCRIPTION OF THE DATA

The observations used in this study, taken with HST/ACS (GO Program 10248), and the photometry with the package DOLPHOT<sup>2</sup> is thoroughly presented in Paper I. These observations cover an area of about  $5' \times 5'$  wide from imaging of three overlapping ACS fields observed with the Wide-Field Channel (WFC) of the camera centered on NGC 346 (Table 1 of Paper I) in the filters  $F555W$  and  $F814W$  ( $\equiv V, I$ ). The  $F814W$  image of the whole field is shown in Fig. 1 (left). This area covers the intermediate-age cluster BS 90 (Bica & Schmidt 1995), the association NGC 346, and all known com-

ponents of the bright nebula N 66, also known as DEM L 103 (Davies, Elliott & Meaburn 1976). The field covering the central area, at RA (J2000) =  $00^{\text{h}}59^{\text{m}}07^{\text{s}}$ , DEC (J2000) =  $-72^{\circ}10'31''$ , was also observed in the narrow-band filter  $F658N$ , equivalent to  $H\alpha$  (“Advanced Camera for Surveys Instrument Handbook” Ver. 7, Oct 2006) with three 512s exposures (Fig. 1, right). In the present study we used DOLPHOT to obtain photometry from the  $H\alpha$  images, and to combine the results with our  $V$  and  $I$  photometry (see § 5).

### 2.1. The Color-Magnitude Diagram of NGC 346

Based on star counts performed in Paper I, we identified the areas where stars of different types are concentrated. The isodensity contour maps from counting the bright upper main sequence (UMS) and PMS stars are shown in Fig. 2. In Paper I these maps allowed the identification of the region which is covered by the association alone. This region is confined within a radius of about  $0.6$  around the geometric center of the system. The  $V-I$ ,  $V$  Color-Magnitude Diagram (CMD) of the stars detected in this region, as the most representative of the association NGC 346, is shown in Fig. 3. This CMD is characterized by a very bright upper main sequence and a prominent sequence of PMS stars, both contaminated by the stellar content of the general field of the SMC, but also of the second dominant stellar concentration, the cluster BS 90. We also identified the area covered by the latter, which is the subject of the second part of our study (Rochau et al. 2007). The part we present here deals with the recent star formation of this active region, and thus it focuses on the young populations as they are revealed from the bright UMS and the faint PMS stars found by our photometry.

### 2.2. Completeness

The photometric completeness is defined as a function of magnitude for both  $V$  and  $I$  band by artificial star experiments described in Paper I. In Fig. 2 of Paper I the “overall” completeness functions for the whole observed stellar sample are shown. Here, we show the completeness factors for the region

<sup>2</sup> The ACS mode of DOLPHOT is an adaptation of the photometry package HSTphot (Dolphin 2000). It can be downloaded from <http://purcell.as.arizona.edu/dolphot/>.

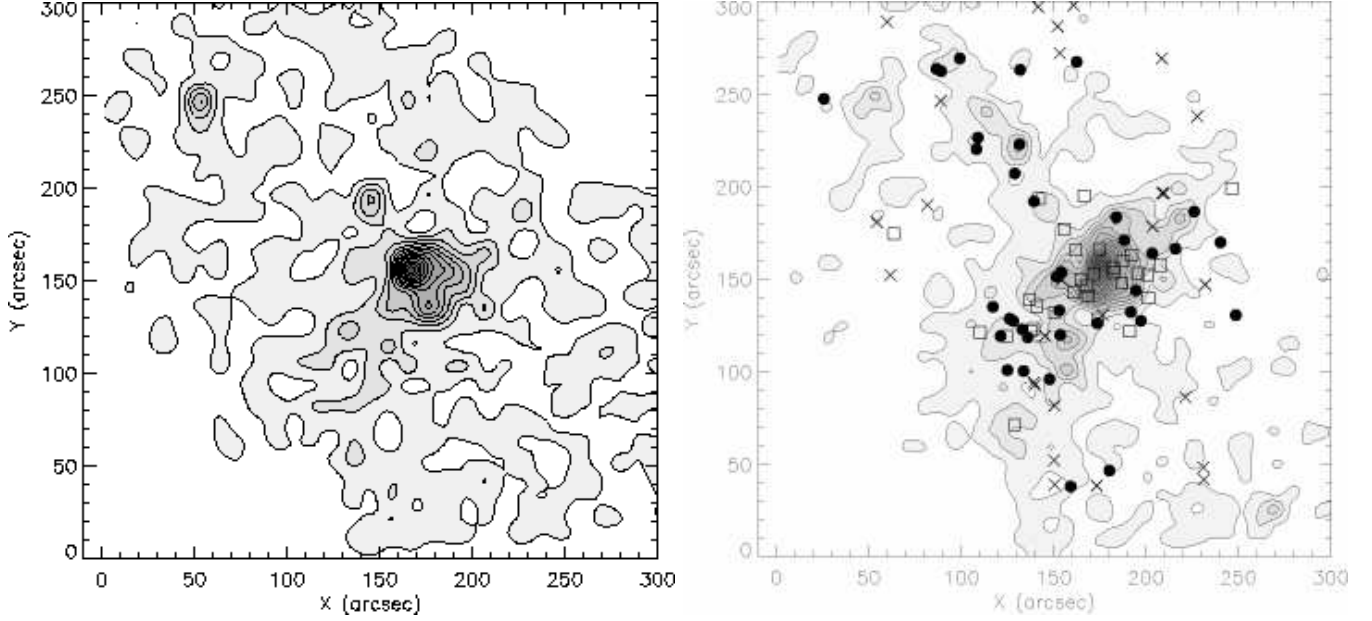


FIG. 2.— Isodensity contour maps constructed from star counts of Upper Main Sequence (*left*), and Pre-Main Sequence (*right*) stars, as they have been selected in Paper I according to their distinct positions in the CMD. The lowest isopleth corresponds to the background surface density and isopleths of higher surface density are plotted in steps of  $1\sigma$ , where  $\sigma$  is the standard deviation of the background density. On the right, the positions of candidate YSOs found in the  $S^3MC$  Spitzer Survey in the observed area around NGC 346 (Simon et al. 2007) are also plotted with crosses and dots, while the brightest 31 OB stars, spectroscopically verified by Massey et al. (1989), included in our photometry are plotted with open boxes. North is up and east to the left on the map.

TABLE 1

PHOTOMETRY OF OB STARS IN NGC 346 BY MASSEY ET AL. (1989), AND FROM OUR ACS ANALYSIS. COLORS AND SPECTRAL TYPES ARE ALSO TAKEN FROM MASSEY ET AL. (1989). THE CORRESPONDING REDDENING FREE PARAMETERS  $Q$  AND THE DERIVED INDIVIDUAL UN-REDDENED COLORS, COLOR EXCESSES AND EXTINCTIONS ARE ALSO GIVEN. STAR ID NUMBERS AND CELESTIAL COORDINATES (IN J2000) ARE FROM OUR CATALOG PUBLISHED IN PAPER I. UNITS OF DECLINATION ARE DEGREES, ARCMINUTES, AND ARCSECONDS; UNITS OF RIGHT ASCENSION ARE HOURS, MINUTES AND SECONDS.

No	RA	DEC	$V_{ACS}$	$V_{CTIO}$	$(U-B)_{CTIO}$	$(B-V)_{CTIO}$	Sp. Type	$Q$	$(B-V)_0$	$E(B-V)$	$A_V$
2	00:59:04.46	-72:10:24.49	12.44	12.57	-1.09	-0.20	O5.5If	-0.95	-0.31	0.11	0.37
5	00:59:00.72	-72:10:27.91	13.52	13.50	-1.12	-0.23	O3V((f*))	-0.95	-0.32	0.09	0.28
6	00:59:00.01	-72:10:37.67	13.69	13.66	-1.05	-0.23	O5.5V	-0.88	-0.29	0.06	0.20
9	00:58:57.36	-72:10:33.38	13.98	14.02	-1.05	-0.24	O4V((f))	-0.88	-0.29	0.05	0.16
10	00:59:01.77	-72:10:30.94	14.38	14.18	-1.08	-0.23	O5.5V((f+))	-0.91	-0.30	0.07	0.24
13	00:59:06.71	-72:10:41.02	14.65	14.53	-1.01	-0.22	O6.5V	-0.85	-0.28	0.06	0.20
14	00:59:06.31	-72:09:55.84	14.37	14.26	-0.91	-0.10	B0.5V	-0.84	-0.28	0.18	0.57
15	00:59:02.88	-72:10:34.68	14.45	14.39	-1.08	-0.22	O7V	-0.92	-0.31	0.09	0.28
18	00:59:14.50	-72:11:59.53	14.97	14.98	-0.90	-0.16	B0V	-0.78	-0.26	0.10	0.32
19	00:59:28.75	-72:10:16.28	15.09	15.14	-0.95	-0.08	B0V	-0.89	-0.30	0.22	0.69
20	00:59:12.28	-72:11:07.66	14.79	14.68	-0.96	-0.19	O7V	-0.82	-0.27	0.08	0.27
21	00:59:12.66	-72:11:08.84	14.85	14.52	-0.96	-0.17	O8V	-0.84	-0.28	0.11	0.35
24	00:59:18.58	-72:11:09.64	14.96	14.87	-1.02	-0.24	O8V	-0.85	-0.28	0.04	0.13
26	00:59:07.29	-72:10:25.10	15.09	15.13	-0.95	-0.30	O8V	-0.73	-0.24	0.00	0.00
27	00:59:05.86	-72:10:50.09	15.01	15.10	-1.00	-0.31	O8V	-0.78	-0.26	0.00	0.00
29	00:59:01.86	-72:10:43.07	15.03	15.03	-1.00	-0.28	O9.5V	-0.80	-0.27	0.00	0.00
30	00:59:12.78	-72:10:52.14	15.18	15.00	-0.93	-0.21	O9.5V	-0.78	-0.26	0.05	0.16
31	00:59:15.48	-72:11:11.44	14.98	14.82	-0.98	-0.15	O6V	-0.87	-0.29	0.14	0.45
32	00:59:09.80	-72:10:58.76	15.25	15.26	-0.96	-0.22	O8V	-0.80	-0.27	0.05	0.15
33	00:59:05.97	-72:10:44.69	15.20	15.04	-0.96	-0.21	B0V	-0.81	-0.27	0.06	0.19
37	00:59:11.61	-72:09:57.31	15.23	14.96	-1.01	-0.16	O5.5V	-0.89	-0.30	0.14	0.44
38	00:58:58.74	-72:10:51.10	15.21	15.20	-0.97	-0.27	O7.5V	-0.78	-0.26	0.00	0.00
39	00:58:58.84	-72:10:38.57	15.20	15.15	-0.97	-0.17	B0V	-0.85	-0.28	0.11	0.36
42	00:59:05.17	-72:10:38.24	15.20	15.20	-1.04	-0.18	B0V	-0.91	-0.30	0.12	0.39
44	00:59:07.59	-72:10:48.07	15.41	15.33	-0.95	-0.24	O6V	-0.78	-0.26	0.02	0.06
48	00:59:04.76	-72:11:02.69	15.39	15.33	-0.87	-0.18	O7.5V	-0.74	-0.25	0.07	0.21
53	00:59:11.88	-72:10:55.56	15.68	15.62	-0.99	-0.20	B0V	-0.85	-0.28	0.08	0.26
54	00:59:00.92	-72:11:09.02	15.60	15.50	-1.03	-0.26	O6.5V	-0.84	-0.28	0.02	0.06
57	00:59:08.65	-72:10:13.87	15.62	15.50	-1.02	-0.28	O7V	-0.82	-0.27	0.00	0.00
65	00:59:02.82	-72:10:37.20	15.63	15.53	-1.02	-0.22	B0V	-0.86	-0.29	0.07	0.21
74	00:58:48.90	-72:09:51.84	15.86	15.85	-0.91	-0.16	B0	-0.79	-0.26	0.10	0.33

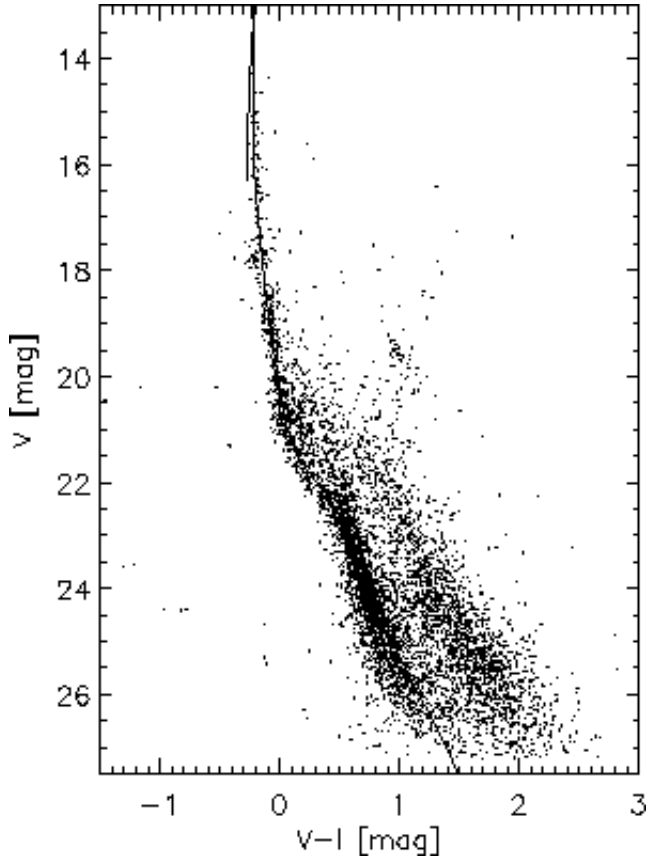


FIG. 3.— The  $V-I$ ,  $V$  Color-Magnitude Diagram (CMD) of the association NGC 346 from HST/ACS photometry. A region within a radius of  $0'.6$  is selected as the best representation of the stellar population, which is characterized by two features in the CMD: the upper main sequence, with 33 spectroscopically confirmed OB stars, and the lower mass Pre-Main Sequence. An isochrone model for an age of  $\approx 4$  Myr Girardi et al. (2002) for  $E(B-V) = 0.08$  mag and a distance modulus  $m-M = 18.9$  mag is overplotted, and confirms the young age of the association.

of the association (Fig. 4), which corresponds to the CMD of Fig. 3. A comparison of the completeness in the area of the association with the overall completeness of the entire region (Paper I) and the one in the area of the cluster BS 90 (Rochau et al. 2007) shows that the association NGC 346 has the lowest completeness. This is not due to higher crowding, since the area of BS 90 is much more crowded, but most probably due to the higher extinction related to this stellar system.

### 2.3. Comparison with previous catalogs

Our photometry also includes the brightest stars in NGC 346. Since the bright main-sequence stars in NGC 346 have been photometrically and spectroscopically studied in detail by Massey et al. (1989), it is worth comparing our results with the ones from these authors. We found, thus, for each star in the Massey et al. (1989) catalog its corresponding record in our catalog. We identified 31 out of a total of 33 bright OB stars for which Massey et al. performed spectroscopy. Our photometry is in excellent agreement with the photometry of these authors, in the sense that their differences are negligible. This is demonstrated in Fig. 5, where the  $V$  magnitudes from CTIO 0.9-m Telescope photometry by Massey et al. and our  $V$  magnitudes from ACS for the 31 common stars are compared (see also Table 1).

### 2.4. Reddening in the observed area

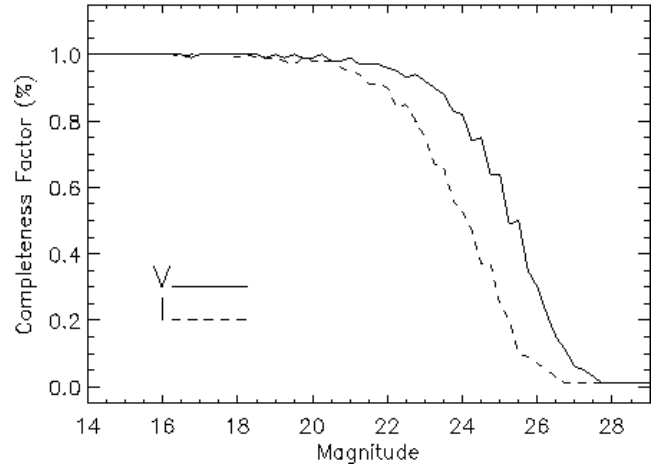


FIG. 4.— Completeness factors as derived by DOLPHOT for all V and I band datasets in NGC 346 within a radius of about  $0'.6$  around its center. Note that due to crowding and the presence of diffuse emission, the completeness is almost one magnitude worse than when considering the entire stellar sample as is shown in Fig. 2 in Paper I.

In order to evaluate the reddening toward different regions of the observed area, we estimated the reddening of individual stars by comparing to “un-reddened” isochrone models. Specifically, the “youngest” available Padova isochrone in the ACS filter system (Girardi et al. 2002) was compared with main sequence stars brighter than  $V \simeq 22$  mag (“upper main sequence” population in Paper I). The observed position in the CMD of each main sequence star with  $V \lesssim 22$  mag was compared to the expected position the star would have according to the Padova isochrone model of  $\log \tau = 6.6$ , assuming that this is the age of the star. Metallicity of  $Z = 0.004$  and a distance modulus of  $m-M = 18.9$  mag, both typical values for the SMC, were considered for the model. The difference between the observed magnitude and color of each star and the values expected by the model provide a measurement of the color excess,  $E(V-I)$ , and extinction,  $A_V$ , for the star. The produced reddening map and the corresponding reddening distribution are shown in Fig. 6. This distribution peaks at  $E(B-V) \simeq 0.08$  mag. The reddening seems to vary from one region to the next and within the boundaries of the association NGC 346 itself, as we show in the next section.

### 2.5. Extinction around the OB stars of NGC 346

Differential reddening is important for the studies of young stellar populations in bright massive stellar systems like NGC 346. In order to quantify the interstellar reddening in different regions within the association, we make use of previous spectroscopic studies of the brightest main-sequence stars observed with our photometry. We have already matched these stars with the OB stars of NGC 346 studied by Massey et al. (1989) (see §2.3). Therefore, we know their exact spectral types. In addition, the  $UBV$  photometry of these authors can be used for estimating the reddening-free parameter  $Q$ :

$$Q = (U-B) - 0.72 \times (B-V)$$

Based on the spectral classification of OB stars in our Galaxy by Schmidt-Kaler (1982) and Peletier (1989) and the photometry of standards of such spectral types by Johnson & Morgan (1953), it is known that the “un-reddened” color index  $(B-V)_0$  is related to  $Q$  by a simple function (Binney & Merrifield 1998):

$$(B-V)_0 \simeq 0.332Q$$

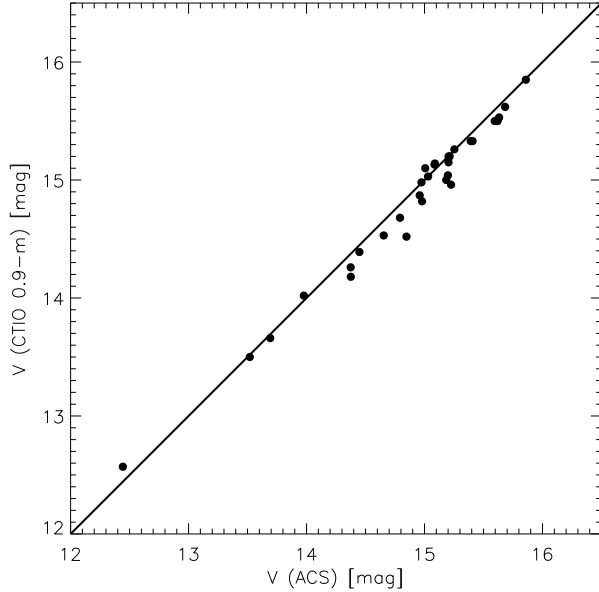


FIG. 5.— Comparison between the  $V$  magnitudes from our photometry with ACS and the photometry with the 0.9-m CTIO Telescope for the 31 brightest OB stars in NGC 346, for which Massey et al. determined accurate spectral types. The drawn line corresponds to the line of excellent coincidence.

We used this relation to estimate  $(B-V)_0$  for each of our OB stars with known spectral types from Massey et al. (1989). Therefore, we are able to estimate their individual color excess  $E(B-V)$  by comparing the observed color indices  $(B-V)$  to their un-reddened ones  $(B-V)_0$ , as calculated from their  $Q$  parameters, and consequently their individual extinction  $A_V$ . The extinction and reddening values found for each OB star are given in Table 1, where it is shown that individual reddening for the OB stars varies from  $E(B-V) \simeq 0.0$  to 0.2 mag ( $0.0 \lesssim A_V \lesssim 0.7$  mag).

The OB stars are centrally concentrated in the association NGC 346 itself, as shown from their spatial distribution in Fig. 2 (right; their positions are indicated by the open boxes), and therefore a comparison between the spatial distribution of their reddening and the one derived from all upper main sequence stars for the whole observed region is not possible. However, typical reddening values derived for the OB stars in the area of the association are found to be systematically lower than those derived in the previous section from upper main sequence stars in the same location. Moreover, the reddening found for the OB stars follow a normal number distribution peaked at  $E(B-V) \simeq 0.04$  mag, which is half of the one found from the upper main sequence stars of the whole region (shown in Fig. 6). From the spatial distribution of the reddening derived from the OB stars, we find that  $A_V$  is higher in the inner parts of the association with values between  $A_V \simeq 0.2$  and 0.4 mag ( $E(B-V) \simeq 0.06 - 0.12$  mag). A possible explanation for the lower reddening toward the OB stars is that probably strong winds from these stars have blown away the gas around them, and therefore reddening appears lower in their vicinities. Considering that the reddening estimation in the previous section is based on a larger statistical sample of stars than the one presented here only for the OB stars, in the subsequent analysis we assume a mean interstellar reddening of  $E(B-V) \simeq 0.08$  mag, a result which also agrees with the one derived for the same region by Sabbi et al. (2007).

### 3. PRE-MAIN SEQUENCE STARS IN NGC 346

The ages of low-mass PMS stars are usually determined from their location in the CMD by comparison to theoretical isochrones (e.g. Briceño et al. 2007). Quite often, a widening of the observed PMS in the CMD gives evidence for an age spread (Palla & Stahler, 2000). However, this spread could also occur because of several other factors which can cause considerable deviations of an individual star's position in the CMD from the location predicted by theoretical models. Such factors include variability, binarity, and the distribution of distances along the line of sight. According to Shu's et al. (1987) picture of star formation a typical galactic molecular cloud could sustain star formation for a timescale on the order of the diffusion time,  $\sim 10^7$  yrs, and an observable consequence would be an age spread in star forming regions, with age of PMS stars comparable to this timescale. Still, as Briceño et al. (2007) reports, no evidence for a wide age spread has been found in the PMS populations of  $\sigma$  Ori, Ori OB1,  $\lambda$  Ori and Upper Sco in our Galaxy. These authors conclude that the data from these different star forming regions support the hypothesis that star formation occurs fast and synchronized in molecular clouds. *Do we observe the same behavior in star-forming regions of the MCs like NGC 346/N 66 based on our ACS photometry of its PMS population?* In the following paragraphs we explore this question.

#### 3.1. Location of PMS Stars in the CMD

In the CMD a well populated faint red sequence of PMS stars is present (Fig. 3). The location of the PMS stars in NGC 346 is in good agreement with the PMS location identified in LH 52 in the LMC (Gouliermis et al. 2006a). The faintest red part of the CMD of NGC 346, where these stars are located, is shown in Fig. 7. The whole stellar sample is plotted in this CMD, with the points corresponding to the stars confined within the region of the association ( $\sim 0.6$  around the center of NGC 346) being plotted with thicker symbols. In the left panel the tentative limits that were selected in Paper I to distinguish the PMS stars from other stellar types are drawn, while in the right panel PMS isochrone models for ages between 0.5 and 15 Myr from Siess et al. (2000) are overplotted. We assume a distance modulus of  $m-M = 18.9$  mag and, although typical value for the metallicity of the SMC is  $Z = 0.004$ , we use PMS models for metallicity of  $Z = 0.01$ , because it is the lowest available in the Siess et al. grid of models. A mean reddening of  $E(B-V) = 0.08$  mag (§ 2.4) was assumed.

#### 3.2. Broadening of the PMS stellar sequence

It has previously been suggested that the PMS stars of NGC 346 represent a single star formation event that took place 3 - 5 Myr ago (Nota et al. 2006). However, a widening of the sequence of PMS stars is apparent in the CMD of Fig. 7. Comparison with theoretical isochrones indicates that it could correspond to an age spread of  $\approx 15$  Myr (Fig. 7, right panel). This suggests that the stars may not be the product of a single star formation event, but instead star formation lasted much longer in NGC 346. In the following, we test this hypothesis and discuss the observational limitations and physical effects, which apart from an age spread can produce the observed broadening of the PMS distribution. Specifically, we analyze how photometric uncertainties, stellar variability, unresolved binarity and variable extinction affect an observed sequence of PMS stars. The individual effect of each of these factors, but also their cumulative effect on the CMD is discussed.

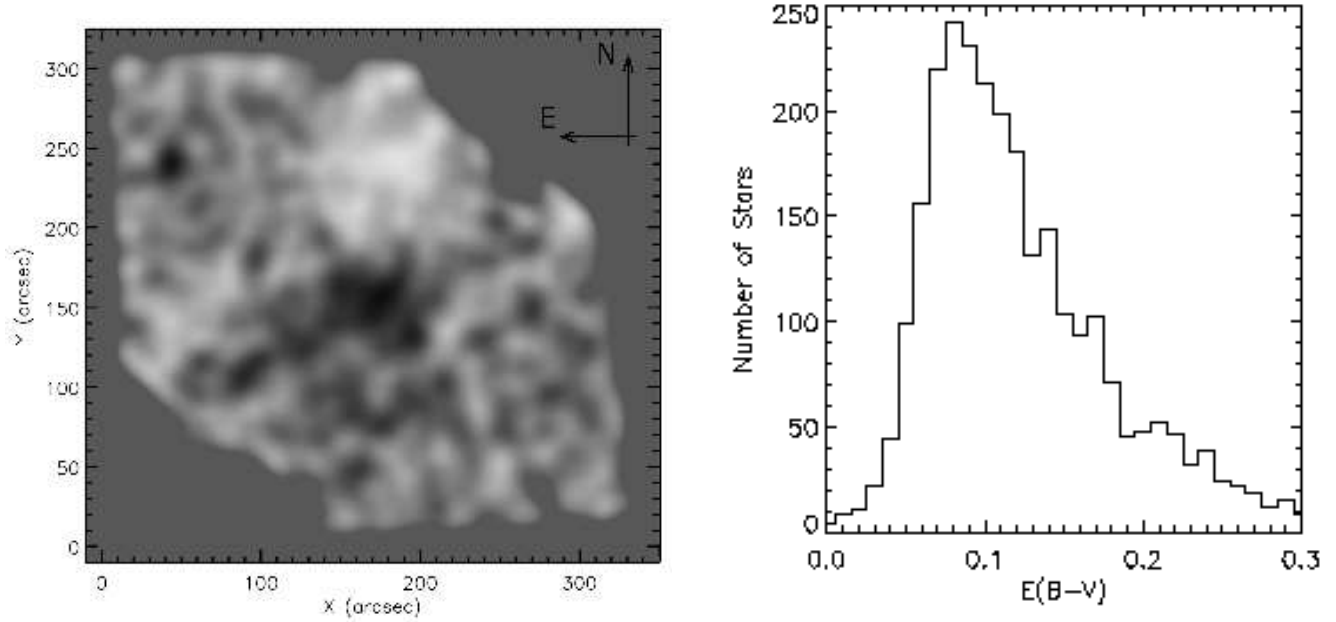


FIG. 6.— *Left*: Reddening Map around NGC 346. This map is based on the upper main sequence stars down to  $V = 22.15$  mag, as they were selected in Paper I. The reddening for each star was estimated by comparison to a Padova isochrone for an age of  $\approx 4$  Myr (Girardi et al. 2002). Darker regions, indicating high reddening, are apparent in the general region of the association and along the related molecular filaments of the N 66 “bar”. The white area to the north corresponds to the cluster BS 90, where no upper main sequence stars are found (Rochau et al. 2007), and therefore there is no reddening measurement for this area. This map also demonstrates the patchy behavior of the reddening further away from the association. *Right*: The reddening distribution from the upper main sequence stars, as it is estimated from comparison with isochrone models. The peak corresponds to color excess  $E(B-V) \simeq 0.08$  mag.

### 3.2.1. Photometry errors

Typical DOLPHOT photometry errors, derived from the PSF fitting, are shown on the right panel of Fig. 7 to illuminate the dependency of the color uncertainties on the brightness of the detected PMS stars. The errors derived from the incompleteness are significantly lower than the photometry errors, and therefore are not considered here. A reasonable explanation for the observed widening of the distribution of the PMS stars could be their photometric errors. However, the observed broadening is wider than the mean photometric errors per magnitude range. For stars with  $V \lesssim 23.5$  mag the sequence of PMS stars is found to cover a color range of at least  $5\sigma$  or more ( $\sigma$  being the typical color uncertainty), while for fainter stars with  $23.5 \lesssim V \lesssim 25.5$  mag, this range becomes at least  $3\sigma$  wide. This implies that the photometric errors alone cannot account for the observed spread in the whole magnitude range of the PMS stars.

### 3.2.2. Binarity

Another factor expected to move PMS stars away from the colors and magnitudes predicted by models is their binarity. Using the simulations of the PMS population with  $24 \leq V \leq 27$  mag and  $1.0 \leq V-I \leq 2.2$  mag of  $\sigma$  Ori by Sherry et al. (2004), we expect at the distance of NGC 346 ( $m-M \simeq 18.9$  mag) a brightness spread of  $\Delta V \simeq 0.75$  mag. The difference in magnitudes between the PMS models for 1.5 and 15 Myr, for the same magnitude and color limits, is  $\Delta V \simeq 2.5 - 1.6$  mag, at least twice as large as the spread produced by binarity.

### 3.2.3. Variability

It is almost certain that the PMS stars of NGC 346 are T Tauri stars, as can be seen from a comparison of their loci in the CMD with the location of T Tauri stars observed, for

example, in the Orion OB1 association in the Milky Way (Briceño et al. 2005). These stars are known to exhibit optical variability, that could cause the PMS spread observed in our CMD. The variability in the  $V$ -band for Classical T Tauri stars (CTTSs) shows an amplitude up to 3 mag, while for Weak-line T Tauri stars (WTTs) the variability is between 0.05 and 0.6 mag (Herbst et al. 1994). In young (3 - 5 Myr) star forming regions the ordinary fraction for CTTSs is 30% - 50% (Preibisch & Zinnecker, 1999), but this fraction decreases with age so that by an age of a few Myr most low-mass PMS stars are WTTs (Sherry et al. 2004). If we assume that this region is indeed very young, then we should consider that no more than 50% of the T Tauri stars in our sample are CTTSs. These PMS stars are characterized by irregular photometric variability (e.g. Sherry 2003) and therefore it is quite difficult to estimate the probability of observing them near the extreme limit of their variability. On the other hand, the photometric variability of these objects is extremely rapid (e.g. Sherry 2003) and consequently the probability of observing its extreme limit is very low. Under these circumstances, a percentage of about 50% of CTTSs in our sample can only partly account for the observed spread. If we consider that the region is older, as suggested by Massey et al. (1989;  $\sim 12$  Myr), then the probability that the observed widening due to variability is even smaller, since these stars would be mostly WTTs.

### 3.2.4. Reddening

Differential reddening is probably the most important factor that might produce the observed broadening. In § 2, we derive the individual interstellar reddening for each of the OB stars within the association. This leads to an estimation of their color excess  $E(B-V)$  and consequently their individual extinction  $A_V$  from their un-reddened color indices  $(B-V)_0$ , and reddening-free  $Q$  parameters (§ 2.5; Table 1). We find that

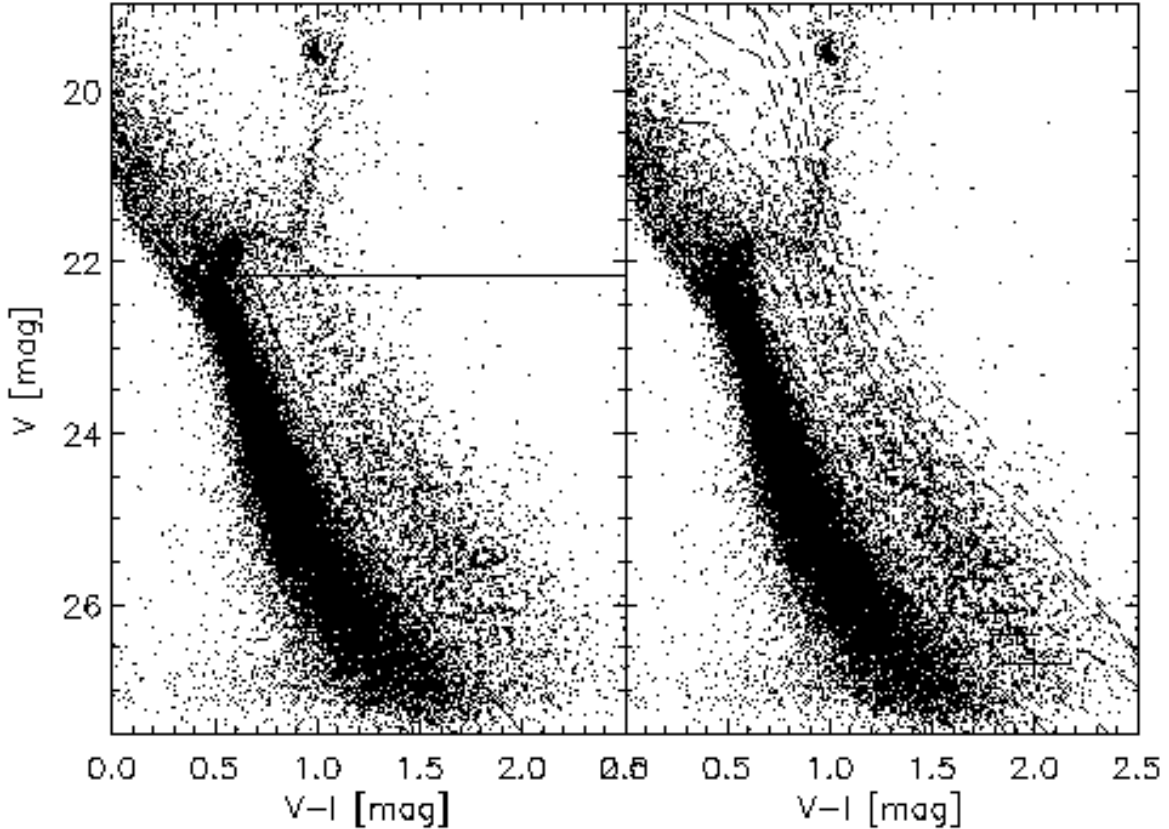


FIG. 7.—  $V-I$ ,  $V$  Color-Magnitude Diagram (CMD) of all stars detected in the area of NGC 346 with ACS imaging, centered on the region of the observed PMS stars. The plot in the left panel shows the area selected in Paper I as the best representative of these stars. In the right panel PMS isochrones by Siess et al. (2000) for ages of 0.5, 0.75, 1.0, 1.5, 2.5, 5, 10 and 15 Myr are overplotted. In both plots the stars confined in an area with radius of about 0.6 around the center of the association are shown with thicker symbols. The ZAMS is drawn as a solid line. DOLPHOT fitting errors in color and magnitude are also shown. The PMS models predict PMS stars well above the limit of  $V \simeq 22$  mag, but the contamination by the background field and mostly by the close-by intermediate-age cluster BS 90 does not allow us to distinguish the PMS stars from the evolved ones for this magnitude range. The wide range of the isochrones which fit the loci of the PMS stars suggests multi-epoch star formation. However the observed broadening of the PMS stars in the CMD might also be the result of several other factors, most prominently among them differential reddening (see text in §3).

extinction varies from  $A_V \simeq 0.06$  to 0.39 mag (with a peak at  $A_V \sim 0.13$  mag). Such an extinction-spread corresponds to a spread in color excess between  $E(V-I) \simeq 0.03$  and 0.20 mag, which is much smaller than the observed widening in color of the sequence of PMS stars. On the other hand, if we consider the reddening distribution based on the upper MS stars of the entire observed region (Fig. 6;  $\langle E(B-V) \rangle \sim 0.08$  mag), then reddening becomes a very important factor for the observed PMS broadening. A further support to the crucial role of reddening is given by the comparison of the spatial variations in the locus of the PMS stars with the reddening map of the observed region derived in § 2.4 (shown in Fig.6 left) and the spatial variations of the reddening of the central 31 OB stars (§ 2.5). This comparison shows that indeed the PMS stars located in the more reddened areas seem to occupy a preferentially redder locus in the CMD. The importance of reddening is demonstrated below with the use of simple simulations of the observed loci of PMS stars in the CMD.

### 3.3. Simulation of the Observed PMS Broadening

We discussed above several factors that may explain the observed PMS spread in NGC 346, and we find that none of them can actually produce this spread in the observed degree *if it acts alone*. However, one should consider that these factors are not isolated phenomena, but, on the contrary, they are expected to act on the observed stellar parameters in a cumulative manner. Taking this into account, we simulate

the observed widening of the PMS assuming that the “suspected” factors act in an additive way on a sequence of single-age PMS stars. We constructed a toy model of the observed PMS stars, assuming that all stars are the product of a single star formation event. Then, we applied each of the aforementioned biases. We conclude from this test that a single-aged PMS population can indeed be misinterpreted as the product of star-formation events that took place during different periods. The apparent age spread can be the product of the cumulative action of several factors.

An example of the results of our toy model is given in Fig. 8, where we assume that the observed PMS population of NGC 346 is 4 Myr old. First, we assume a concentration of PMS stars, as they are selected in Paper I according to their location in the CMD (Fig. 8a), which populates a single 4 Myr PMS isochrone (Fig. 8b). Then we apply the effects of the suspected factors one on top of the other. Here we describe the procedure:

- (i) *Binarity*: As far as the existence of unresolved binaries in our sample concerns, there are no studies on the expected fraction of binary systems in associations of the Magellanic Clouds. Therefore, we based our simulations on the information we have on galactic OB associations. These systems show a binary fraction that does not differ significantly from the field (Mathieu 1994), which is found for G dwarfs to be around  $\sim 58\%$  (Duquennoy & Mayor 1991). The well-studied Orion

Nebular Cluster (ONC) is also found to be consistent with the field binary fraction (e.g. Prosser et al. 1994; Petr et al. 1998; Köhler et al. 2006). In many clusters, a clear binary sequence is observed to lie 0.75 magnitudes above the single star main sequence (Tout 1991), and this is almost equal to the brightness shift that a single star will suffer toward brighter magnitudes, if it is an unresolved binary system with equal mass components (de Bruijne et al. 2001).

Simulations of unresolved low-mass PMS stars in the Orion OB1b association centered on  $\sigma$  Ori by Sherry (2003) showed that for a 3 Myr old binary system with a  $0.5 M_{\odot}$  primary the position of the system on the  $V-I$ ,  $V$  CMD can be shifted up to 0.13 mag on the  $V-I$  axis. The actual shift depends on the mass of the lower-mass companion, which ranges from 0.1 to  $0.5 M_{\odot}$ . This system also brightens by slightly less than 0.75 magnitudes. It should be noted that recent observational studies on the mass ratios of T Tauri binaries are consistent with a uniform distribution of mass ratios between 0.2 and 1.0 (Woitas et al. 2001). In order to simulate the effect of unresolved binaries to the modeled sequence of 4 Myr old PMS stars we randomly applied a brightening of no more than  $V \simeq 1$  mag and a reddening  $\lesssim 0.13$  mag, assuming different binary fractions. It is worth noting that Elson et al. (1998) measured a binary fraction in the young rich LMC cluster NGC 1818, and found  $35 \pm 5\%$  in the core. This is roughly comparable to the Galactic values which are considered here. In Fig. 8c (top panel) the result for a binary fraction of 50% is shown. This result clearly suggests that binarity can play an important role to the broadening of a single-age PMS population in the  $V-I$ ,  $V$  CMD.

- (ii) *Variability*: In order to simulate the effect of variability on our modeled sequence of PMS stars, we assigned to each star a random amplitude drawn from a Gaussian probability distribution, following Sherry (2003), who assumed normally distributed  $V$ -band variations in WTTs with a mean of  $M_V = 0.15$  mag and a standard deviation of  $\sigma = 0.1$  mag, based on data for 42 WTTs with known  $V$ -band variations. The  $V-I$  colors of these stars should appear redder when they are fainter, due to rotational modulation. According to Herbst et al. (1994) the ratio of color variations,  $\Delta I / \Delta V$ , ranges from 0.39 to 0.88 mag. We assumed several values for this ratio within these limits. In Fig. 8d (top panel) we show the results assuming a mean value of  $\Delta I = 0.6 \Delta V$  and consequently  $\Delta(V-I) = 0.4 \Delta V$ . It should be noted that for these results we assumed that only WTTs are present at the assumed age of NGC 346. This is certainly the reason for a rather small effect on the variability in our simulations. In the case that some fraction of CTTSs had also been included, the spread implied by the model could be as large as 5 times more, due to the higher amplitude these stars exhibit.
- (iii) *Reddening*: We explore the displacement of the PMS stars from their theoretical loci on the CMD due to reddening. We assume that these stars are subject to a) the reddening of the whole area as estimated from the upper main sequence stars (§ 2.4), by randomly applying the observed reddening distribution shown in Fig. 6 (right), and b) the much lower reddening of the area of

NGC 346 alone found from the OB stars (§ 2.5). For Fig. 8e (top panel), the assumed reddening distribution was based on stars in the whole region with  $V \lesssim 21$  mag, and is chosen to show the maximum effect. The corresponding distribution for even brighter stars is thinner with smaller mean values and standard deviations. This would also be the result for the (more accurately measured) reddening found for OB stars. As shown in Fig. 8e, high extinction is indeed the most important factor, in addition to binarity, that can cause the observed broadening of single-age PMS stars.

- (iv) *Photometry*: Photometric accuracy is a function of magnitude, being higher for the brighter stars. In order to explore the effect of photometric uncertainties to a “perfect” sequence of PMS stars, we randomly applied the observed mean photometric errors per magnitude (shown in Fig. 7 right) to the modeled PMS population. Naturally, the derived broadening is wider for the fainter stars. This is shown in Fig. 8f (top panel).

From the results of our toy model for the influence of several factors on a “perfect” single-age sequence of PMS stars, it can be seen that indeed a single-age PMS population may appear broad enough in the  $V-I$ ,  $V$  CMD so that it could be misinterpreted as a group of stars, produced by multi-epoch star formation. We specifically note the importance of reddening and binarity of such stars for this broadening. Variability may also play an important role depending on the nature of these stars. Although each of these factors acting alone cannot cause the observed widening of PMS loci in the CMD, it is their cumulative action that leads to the broadening of the sequence of PMS stars in NGC 346. However, it should be noted that if indeed reddening is the most important cause for this widening, then the PMS population of NGC 346 should be expected to be older than 3 - 5 Myr, since reddening “pushes” PMS stars to redder colors making them appear *younger*. Specifically, PMS models for ages on the order of 10 Myr proved to fit the observed sequence of PMS stars and their broadening better. This result is in line with Massey et al. (1989), who claim that although the location of the bright stars of NGC 346 in the CMD implies an age of less than 5 Myr for the association, there is a spatial distinct subgroup of evolved  $\sim 15 M_{\odot}$  stars *in the association* with ages  $\simeq 12$  Myr.

Furthermore, another very interesting result of our simulations is that the possibility of multi-epoch star formation cannot be excluded. Specifically, our toy model showed that if we consider that the interstellar reddening may be lower than what was previously assumed (using e.g.  $E(B-V) \simeq 0.04$  mag found from the OB stars in the region of the association), then the observed spread of the PMS stars can only be reproduced by (at least) two separate PMS isochrones. This is demonstrated in Fig. 8 (bottom panel), where we show the results of the toy model if two star formation events around 4 and 10 Myr ago are assumed. In this figure it is shown that the final broadening of the PMS loci in the CMD does not differ significantly (although it is a bit wider) from the one resulted from a single star formation event. Typical ages derived from the simulations of a double star formation event (half of the stars formed in each epoch) are 3 - 4 and 10 - 12 Myr in agreement with both hypotheses. Conclusively, we *cannot* completely exclude the possibility of a true age spread of the sequence of PMS stars in NGC 346 due to separate star formation events.



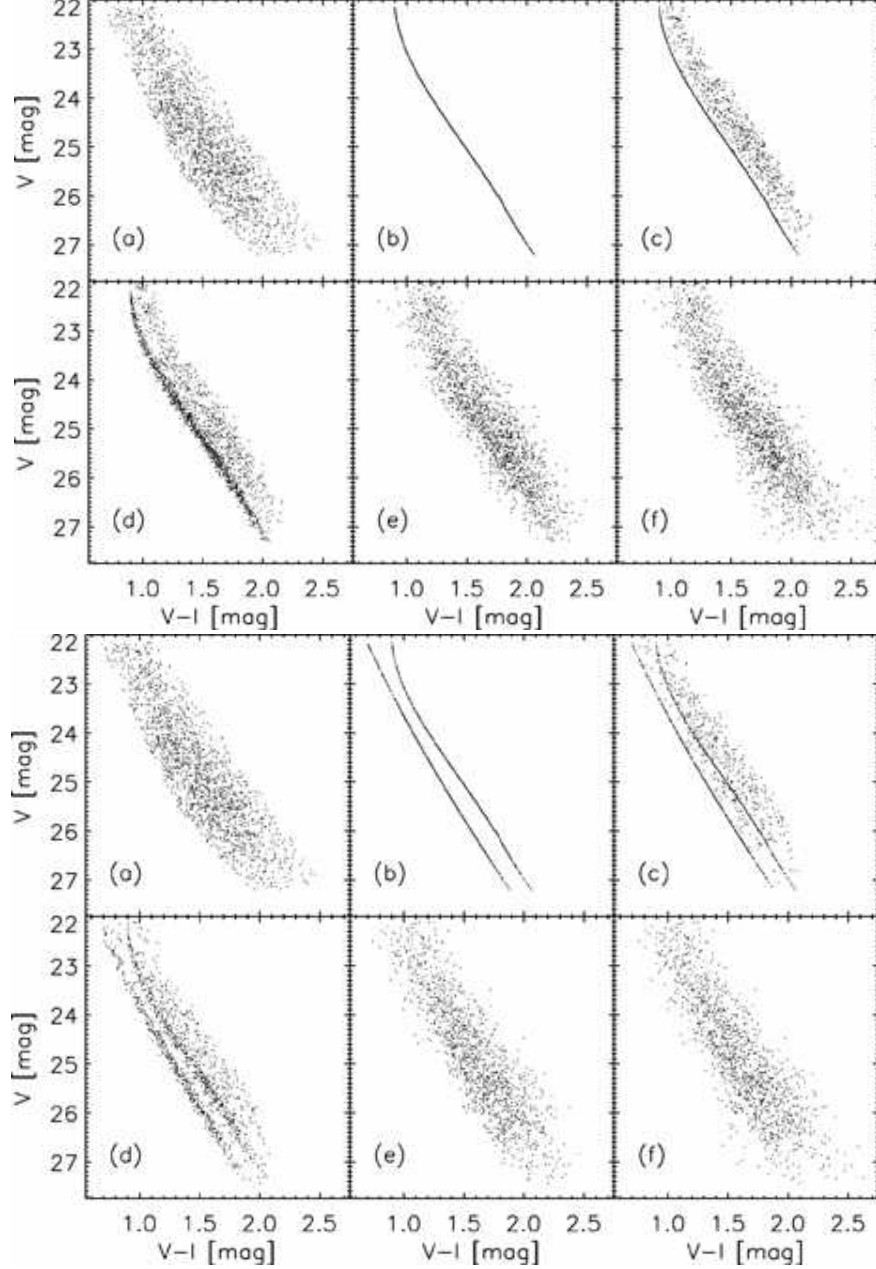


FIG. 8.— *Top*: An example of the results from our toy model used to simulate the cumulative effect of several factors on a single-age sequence of PMS stars. (a) The observed PMS stars in the region of NGC 346 are selected according to their positions in the  $V-I$ ,  $V$  CMD. (b) Their positions are modeled based on the 4 Myr PMS isochrone from Siess et al. (2000). Factors, such as (c) binarity, (d) variability, (e) reddening and (f) photometric uncertainties are applied in order to explore the broadening they cause to a single-age PMS population, making it appearing as the result of multi-epoch star formation (see § 3.3). *Bottom*: Results from a toy model similar to the one on the top, but assuming that the PMS stars are formed during two star formation events, one 10 Myr and the other 4 Myr ago. In this example 50% of the population is assumed to be formed during the first and 50% during the second event. These results imply that the possibility of more than one star formation events in NGC 346/N 66 cannot be ruled out.

#### 3.4. CMD Variations within the Region of NGC 346

In order to study variations in the CMD we selected a region of size  $1'.5 \times 1'.2$ , centered on the association NGC 346. This region was divided into 20  $18'' \times 18''$  sub-regions. Indeed, we see that the CMDs differ from one region to the next in the nature of the stars, their numbers and the apparent PMS broadening. The individual CMDs of all sub-regions are shown in Fig. 9. In order to avoid confusion, PMS isochrones are overplotted only for sub-regions 11 to 15, so that a rough estimation of the age differences can be extracted. Specifically, isochrones for 1.5 and 10 Myr are displayed in the CMD of sub-region 11, the 0.75 and 15 Myr isochrones are shown in the CMDs of sub-regions 12 and 13, whereas for the CMD of

sub-region 14 the older age limit seems to be better fit by a 10 Myr isochrone, but for a very low number of faint PMS stars.

From Fig. 9, it can be seen that PMS stars are present in almost the entire selected region, except for the southwestern (sub-regions 5 and 10) and northeastern (sub-region 16) areas, which are located away from the association (and the nebula). From the CMDs of the remaining sub-regions we can conclude that PMS stars seem to follow the southeast (bottom left corner) to northwest (top right corner) direction of the *nebula*, with a higher concentration in the main body of the association (sub-region 13) and around it (e.g. sub-regions 12,

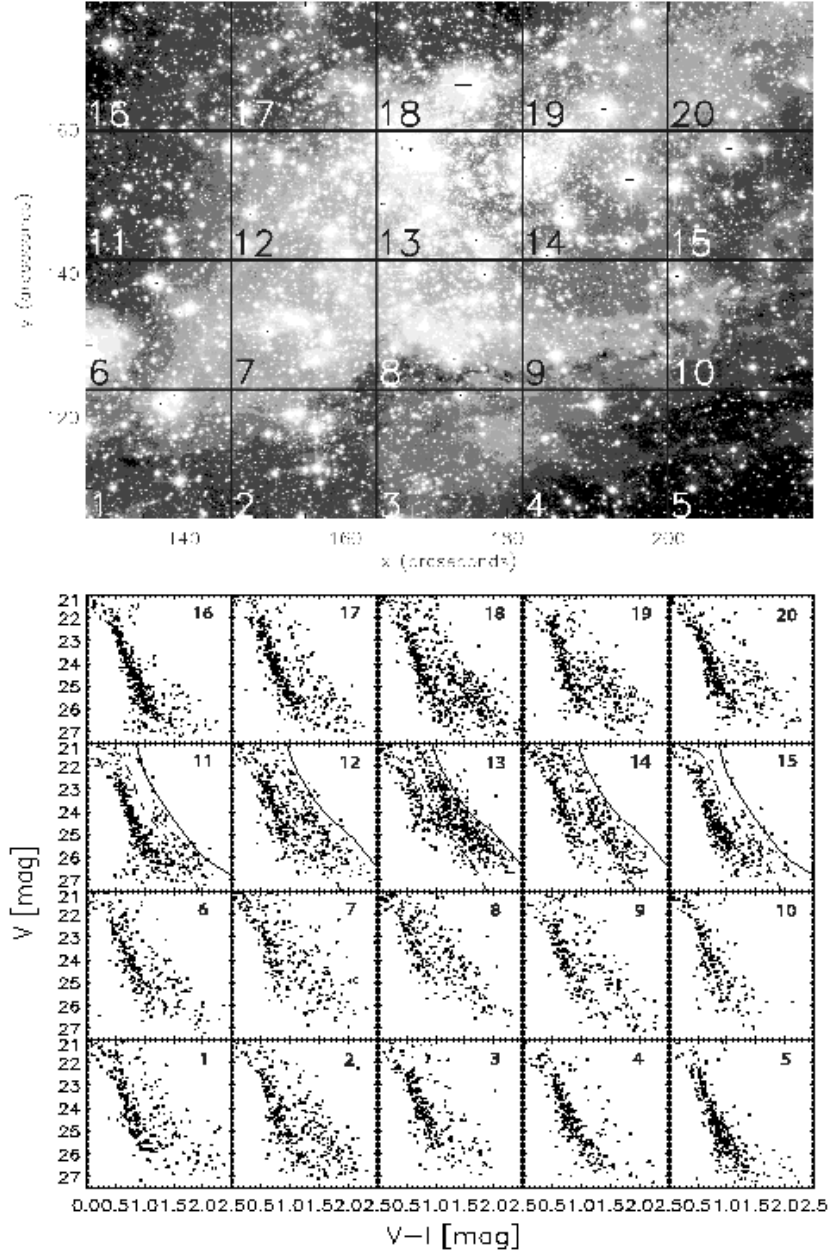


FIG. 9.— *Top*: A  $1\frac{1}{2} \times 1\frac{1}{2}$  region centered on the association NGC 346, with the borders of 20 selected sub-regions  $18'' \times 18''$  wide each overplotted. *Bottom*: The CMDs of the sub-regions, with PMS isochrones overplotted for sub-regions 11 to 15. PMS stars are present in almost the entire region, and they seem to be aligned across the nebula. This plot shows that the CMD varies in number of PMS stars and width of their broadening from one region to the other.

14 and 18)<sup>3</sup>. Reddening in the selected region is expected to be higher in the part centered on the main body of NGC 346 due to the nebula, and indeed the corresponding CMDs exhibit the wider broadening in their PMS populations. This suggests that reddening is indeed (at least partly) responsible for the observed PMS broadening. This is more clearly seen in the CMD of sub-region 13, the best representative of the population of the association (similar to the CMD used in our toy-model).

From the discussion so far on the PMS stars of association NGC 346 alone we *cannot* safely conclude that these stars represent a coherent population, formed in a single star formation event. Nota et al. (2006) and Sabbi et al. (2007) argue

that such an event happened 3 - 5 Myr ago, while Massey et al. (1989) suggest a timescale three times longer, closer to our results presented in §3.3. However, taking into account the low reddening found from the OB stars in the association, we tend to conclude that a true age spread may also contribute to the observed PMS broadening.

NGC 346 does not seem to represent the only product of recent star formation in the general area. As shown from the isodensity contour maps of Fig. 2, density peaks of PMS stars can be seen away from the association, forming small compact concentrations, which we refer to as “PMS clusters”. We also present our results from H $\alpha$  observations and previous results from observations with the *Spitzer* Space Telescope in the mid- and far-infrared, which reveal loci of on-going star

<sup>3</sup> The concentration of PMS stars in sub-regions 3, 4, 5, 10, 11, 15, 16 and 17 is lower than the one along the southeast-northwest axis.

formation in the general region of NGC 346/N 66.

#### 4. PMS CLUSTERS IN THE REGION OF NGC 346/N 66

##### 4.1. The most significant PMS clusters in the Region

The isodensity contour map of the region of NGC 346/N66 constructed from star counts of the PMS stars is shown in Fig. 2 (right panel). In this map several distinct concentrations of PMS stars can be identified. We selected the statistically most significant concentrations with a density  $\gtrsim 3\sigma$  above the background (where  $\sigma$  is the standard deviation of the background density). There are five such concentrations, which fit the description of “PMS clusters”. The contour map of the whole region, as well as the ones of the local regions around each of these clusters, numbered from north to south, are shown in Fig. 10 (top).

The size of each PMS cluster was defined by a closer inspection of their contour map, as shown in Fig. 10 (top). The center was chosen to be the density peak. A circular area was selected to represent the extent of each cluster with a radius determined by the isopleth, corresponding to the mean density of the surrounding region (first isopleth in the individual maps of the clusters). This isopleth defines the size of each cluster. It should be noted that cluster 2 consists of two distinct regions, which we will treat in the following study separately. Clusters 1 and 3 are clearly detected in the contour maps of both PMS and Upper Main Sequence stars (see Fig. 2). Therefore, their size was determined by the contour maps constructed with both PMS and UMS stars. In order to define an age range within which each PMS cluster was presumably formed we construct the CMD of the stars included in the area covered by each cluster.

##### 4.1.1. Color-Magnitude Diagrams of the PMS Clusters

Although it is quite difficult to disentangle the actual age of the discovered PMS clusters, because of the artificial broadening of the PMS loci in the CMD discussed in § ??, it is worthwhile to specify the limits within which their ages may range, in order to identify any age-differences between them. Therefore, the stellar populations of the PMS clusters are analyzed in terms of their CMDs shown in Fig 10 (bottom). Isochrone models for both MS (Girardi et al. 2002) and PMS (Siess et al. 2000) populations are overplotted. These models suggest that cluster 1 is in a rather evolved state with the best fitting PMS model indicating an age range of 5 to 15 Myr. The stellar content of this cluster, which also includes a few bright MS stars, suggests that it should be treated as a small open cluster rather than a recently formed PMS cluster.

The models indicate that all the remaining PMS clusters seem to be much younger than cluster 1. Specifically, clusters 2 to 4 do not exceed an age of 5 Myr, with clusters 2a, 2b and 3 being the youngest in the sample with ages for their PMS stars younger than 2.5 Myr. All isochrone models have been plotted for a mean reddening of  $E(B-V) \simeq 0.08$  mag. Differential reddening is found to play an important role in the broadening of the PMS stars in the CMD. However, a constant mean reddening should be considered for the isochrone models, and we found that the selection of this reddening according to the measurements of § 2.4 and § 2.5 does not seem to be very important for the derived age-span of the clusters. This is demonstrated in Fig 10 for the CMD of cluster 2a, where we plot the PMS isochrones assuming three cases: No reddening (dash-dotted lines) and reddening values of  $E(B-V) \simeq 0.08$  mag (found from the upper main sequence

for the whole region; dashed lines) and  $E(B-V) \simeq 0.04$  mag (found from the OB stars in the association; long-dashed lines).

The spread of the PMS stars in the CMD of cluster 5 covers a wider range of ages, comparable to the one we observe in the main body of the association NGC 346 (discussed in §3). This is not a surprising result considering that cluster 5 is the closest PMS cluster to the association, and probably it shares the same star formation history with it. In general, from the individual CMDs of the PMS clusters (except for cluster 1, which is a rather evolved open cluster with a PMS population) we see that the northern part of the observed field (north of the association) covers younger clusters of PMS stars than in the southern part and the association itself. It will be discussed below whether this is an indication that these clusters do not share the same star formation history with NGC 346, but rather that they are the products of more recent star formation.

##### 4.2. Cluster Properties of PMS Stars

The degree of clustering of PMS stars can be evaluated through their surface density as a function of angular separation from each star. Gomez et al. (1993) applied this technique to the study of the spatial distribution of PMS stars in the Taurus-Auriga molecular cloud, and they found that a power law form (with index  $\gamma \simeq -1.2$ ) reproduces the overall shape of the actual PMS distribution in Taurus, indicating the presence of real clustering. Larson (1995) extended the analysis of Gomez et al. to smaller separations and he measured a power-law relation  $\Sigma \propto \theta^\gamma$  for young star clusters, where  $\Sigma$  is the surface density of PMS stars, and  $\theta$  the angular separation from each star. He found that the Taurus young stars exhibit self-similar or fractal clustering on the largest scales, but there is a clear break from self-similarity at a scale of about 0.04 pc which divides the regime of binary and multiple systems on smaller scales from that of true clustering on larger scales.

A survey of young clusters in the Orion, Ophiuchus, Chamaeleon, Vela, and Lupus star-forming regions by Nakajima et al. (1998) showed an index for  $\Sigma(\theta)$  of  $\gamma \simeq -2$  at stellar separations in the binary regime, smaller than 0.1 pc, whereas at large separations (0.1 to 1.0 pc.), the power index seems to vary from region to region with  $-0.8 < \gamma < -0.1$ . The break in the power law was found to occur on physical scales of 0.01 to 0.1 pc. Pudritz (2002) argues that this spatial range probably does not reflect the initial conditions for isolated star formation in clusters, because a star moving at  $\simeq 1.0 \text{ km s}^{-1}$  in such a cluster will move a distance of 1.0 pc in a million years, thereby erasing the initial conditions. According to Larson, the power law break provides clear evidence for an intrinsic scale in the star formation process, which is found to be essentially equal to the Jeans length in typical molecular cloud cores. He also notes that there is evidence that nearly all stars are formed in binary or multiple systems, and that some of these systems are subsequently disrupted by interactions in the denser star-forming environments to produce the observed mixture of single, binary and multiple stars (Larson 1995). Goodwin et al. (2007) review the observed properties of multiple systems and find that the multiplicity of stars changes, probably due to the dynamical decay of small-N systems and/or the destruction of multiple systems within dense clusters. They note that models of the fragmentation of rotating and turbulent molecular cores almost always produce multiple systems, but the properties of those systems do not match the observations.

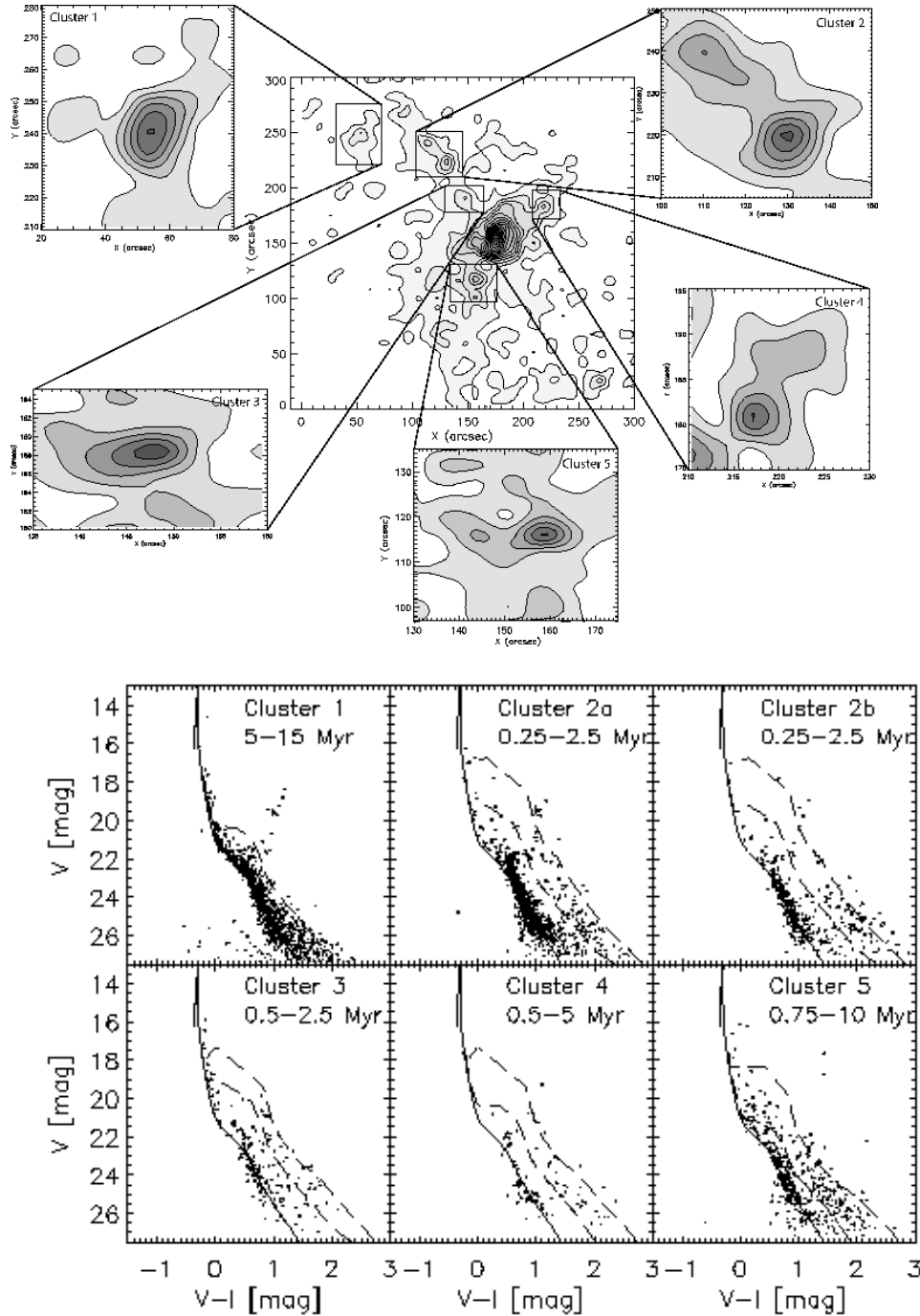


FIG. 10.— Top: Isodensity contour map from star counts of the PMS stars of the area of NGC 346/N 66, as they have been selected in Paper I. Five PMS clusters in the area around the association NGC 346 are selected based on their high density of PMS stars and the corresponding local contour maps are shown enlarged. Bottom:  $V-I$ ,  $V$  CMDs of the stars included within the area of each of the selected PMS clusters. An isochrone for an age of  $\approx 4$  Myr by Girardi et al. (2002) is overplotted for the main sequence populations. For the PMS stars, isochrone models by Siess et al. (2000) are overplotted to indicate the time range within which these stars have presumably formed. Cluster 1 seems to be rather a more evolved open cluster, while cluster 5 meets the characteristics of the association itself. Clusters 2a, 2b and 3 probably represent the youngest products of clustered star formation away from the association NGC 346.

OB associations are known to contain subgroups of smaller clusters (Blaauw 1983), which often contain smaller groups of stars themselves, made of multiple-star systems. Efremov & Elmegreen (1998) suggest that star formation is generally clumped into a hierarchy of structures, from small multiple systems to giant star complexes and beyond and that OB associations are just one level in this hierarchy. Even the ISM has been observed to be arranged in a hierarchical structure (Scalo 1985; Vázquez-Semadeni 2004). Turbulent motions have been proposed as a cause for the hierarchical structure

(Elmegreen 1998). The velocity structure in turbulent regions is suggested to be scale-free, meaning that *the same physical processes and the same velocity-separation relations occur over a wide range of absolute scales* (Elmegreen 2006). According to this hypothesis, large clumps originate from the large velocities which compress the gas on large scales and small clumps result from the compression of the gas characterized by small velocities on small scales. Considering that stars are formed by the collapse of such hierarchical structured clumps, they are themselves hierarchically structured.

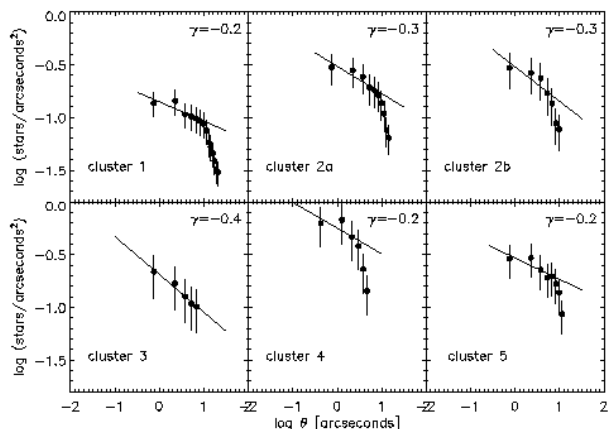


FIG. 11.— Average surface density of companions as a function of angular separation from each star for the PMS clusters identified in the region of NGC 346 (Fig. 10). From our observations we cannot distinguish separations in the binary regime. Therefore, the power-law index is given only for larger separations, typically in the range  $0.8''$  to  $8''$ , corresponding to physical scales of 0.24 pc to 2.4 pc at the distance of the SMC. The fitting functions, presented by solid lines, and the corresponding indices,  $\gamma$ , are given for each cluster. Their values indicate that all PMS clusters should be considered as results of a hierarchical clustering process (see section 4.2).

The break in the power-law relation  $\Sigma \propto \theta^\gamma$  defines the two different regimes of star formation: The binary regime at smaller scales, and the regime of hierarchical clustering at larger ones.

In order to determine the clustering properties of the PMS clusters found in the region of NGC 346, we apply the same technique and construct the average surface density of companions  $\Sigma(\theta)$  for every PMS member of each of the PMS clusters as a function of the angular projected separation  $\theta$  (see Fig. 11). We apply a linear fit for the estimation of the power law index,  $\gamma$ . The function  $\Sigma(\theta)$  drops sharply near the largest separations owing to the size of the region selected for each cluster. Consequently, our analysis is based only on the smaller observed separations. In addition our observations do not allow us to separate stars in the binary regime and, therefore, our study does not include them. The errors shown in Fig. 11 reflect the low number statistics in our samples of PMS stars per cluster.

The derived values of the power-law index for all clusters are found to be in the narrow range  $-0.4 < \gamma < -0.2$ , comparable to the results of Nakajima et al. (1998) for separations in the regime of hierarchical clustering. The power-law index relates to the nearest-neighbor distance, in the sense that if the latter can be fitted by the Poisson distribution, then the power index is close to 0. The distribution of the nearest-neighbor distance is much broader than the Poisson one, when the surface density varies appreciably within the region. Then  $\Sigma(\theta)$  has a steep  $\theta$ -dependence, and the power-law index is negative (Nakajima et al. 1998), comparable to the values we find for our clusters. Consequently, these values can be interpreted as the result of the variation of the surface density within the region, and clearly suggest that the PMS clusters identified in the region of NGC 346/N 66 are the products of hierarchical clustering.

## 5. $H\alpha$ OBSERVATIONS OF THE NGC 346/N 66 REGION

### 5.1. Stars with $H\alpha$ excess

In total, more than 23,000 stars are detected with our photometry in all three  $V$ ,  $I$  and  $H\alpha$  bands with photometric uncertainties less than 0.1 mag. By comparing the  $H\alpha$  and  $R$

magnitudes of the detected sources, one can identify stars with  $H\alpha$  emission (e.g. Grebel et al. 1992, Keller et al. 1999). As our dataset is lacking observations in  $R$ , we determined a “synthetic”  $R$  magnitude for every star derived by accurate interpolation between  $V$ -,  $R$ - and  $I$ -band data for the filter set of ACS, as  $m_{675} = 0.38m_{555} + 0.62m_{814}$  (De Marchi, *private communication*). We identified the  $H\alpha$  emission stars in our sample by plotting the  $R - H\alpha$  color index against case  $V - I$  (see Fig. 12, *left*), and then applying the selection criterion requiring all  $H\alpha$  emission stars to have  $R - H\alpha \geq 0.4$  mag above the sequence of non-emission stars (Keller et al. 1999). This selection revealed 309 stars, which are marked by fat dots in the  $V - I$ ,  $V$  CMD in Fig. 12 (*right*). The bright sources of this sample are candidate Herbig Ae/Be stars or evolved Be stars, while the fainter are T Tauri stars still in their pre-main sequence phase.

### 5.2. Spatial Distribution of Stars with $H\alpha$ Excess

The spatial distribution of the stars with  $H\alpha$  excess coincides with the outline of the HII region (Fig. 1 (*right*) as well as the general spatial distribution of the PMS stars (Fig. 2, *right*) and the infrared emission from *Spitzer* observations (Simon et al. 2007; see also next section). Two major concentrations of emission stars can be readily identified, one located in the nebula N 66, following its general southeast-northwest trend, and the other to the north-northeast part of the association, coinciding with clusters 2a, 2b and 3.

## 6. *SPITZER* OBSERVATIONS OF NGC 346

As part of the *Spitzer* Survey of the Small Magellanic Cloud ( $S^3MC$ ), Bolatto et al. (2007) imaged the SMC in all seven MIPS and IRAC wavebands, and compiled a photometric catalog of 400,000 mid- and far-infrared point sources. A color-composite image from *Spitzer*/IRAC imaging of the general area of NGC 346/N 66, retrieved from the *Spitzer* Data Archive is shown in Fig. 13. Bolatto et al. (2007) identified 282 bright candidate Young Stellar Objects (YSOs) as bright  $5.8 \mu\text{m}$  sources with very faint optical counterparts and very red mid-infrared colors ( $[5.8] - [8.0] > 1.2$  mag, where  $[5.8]$  and  $[8.0]$  are the magnitudes of the sources in the  $5.8 \mu\text{m}$  and  $8.0 \mu\text{m}$  IRAC bands, respectively). 16 of these candidate YSOs fall within the NGC 346 region observed with HST/ACS. By comparison with our ACS photometric catalog (Paper I) we obtained optical photometry for the candidate YSOs. Because of the difference in angular resolution of at least  $\approx 20$  between *Spitzer* and ACS, a unique identification of the optical counterparts of the YSO candidates is not always possible. In Table 2 we summarize the IRAC and MIPS photometry of the YSOs identified by Bolatto et al. (2007) as well as the ACS photometry of the brightest star located within  $1''.5$  of the *Spitzer* position. We also quote the number of stars detected on ACS within this radius, and find evidence for significant clustering. Up to  $\approx 20$  brighter main sequence and fainter pre-main sequence stars can be found within  $1''.5$  of the YSOs, i.e. we might be seeing compact stellar clusters. The mean density of these stars for the whole region ( $\sim 0.15$  stars/ $\square''$ ) is much lower than the average stellar density of the stars found within  $1''.5$  around candidate YSOs. A study of the clustering of PMS stars at the loci of YSOs in the SMC association NGC 602 is presented by Gouliermis et al. (2007). These authors note that high-resolution near-infrared imaging and spectroscopy are required to better understand the stellar populations and clarify if they are signatures of on-going clustered star formation.

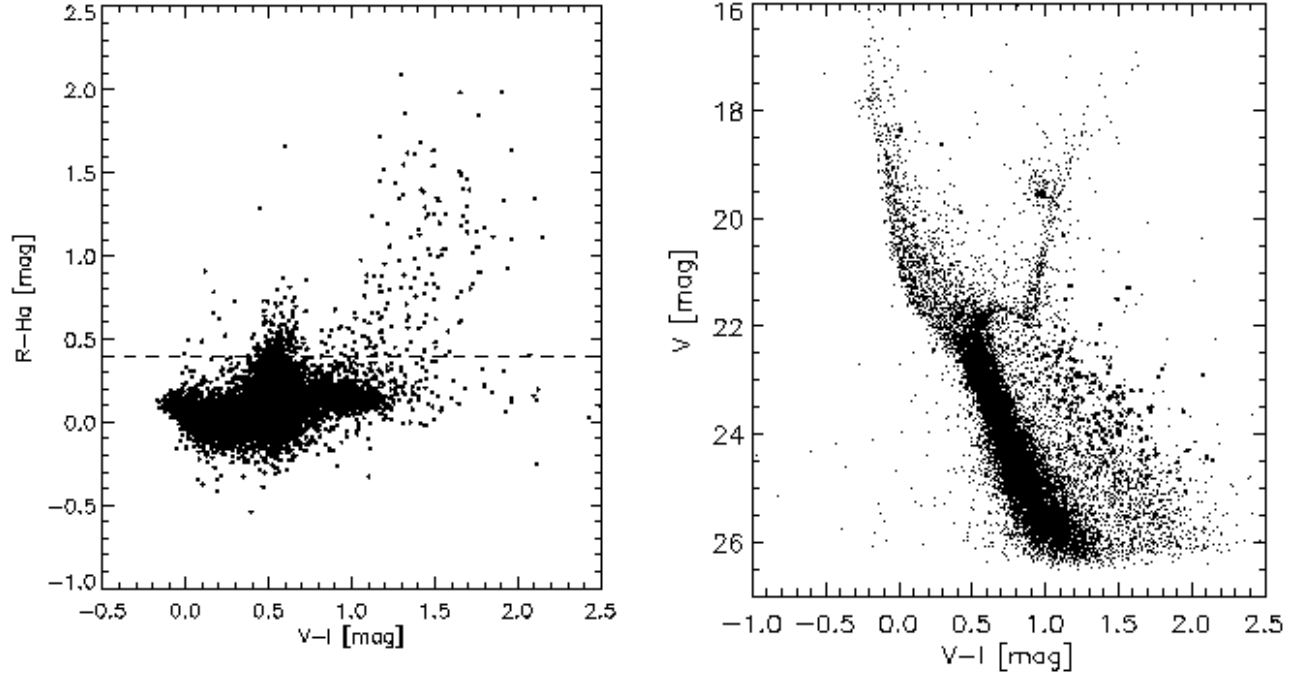


FIG. 12.— *Left*: In a  $R-H\alpha$ ,  $V-I$  color-color diagram stars without  $H\alpha$  emission form an almost horizontal band around  $R-H\alpha \simeq 0.0$  mag, with most of the low main-sequence stars concentrated around  $V-I \simeq 0.5$  mag. The spread of normal MS stars in  $R-H\alpha$  is mostly due to the photometric errors in the narrow-band  $H\alpha$  magnitudes. The group of cooler stars with  $R-H\alpha \geq 0.4$  mag are mostly faint PMS stars, which exhibit  $H\alpha$  excess. Few bright stars with strong  $H\alpha$  emission, which may be Herbig Ae/Be stars, or Be type stars, are also found. *Right*: The  $V-I$ ,  $V$  CMD of all emission line sources (thick symbols) overlaid on the CMD of the whole sample of stars. Both bright and faint PMS stars with  $H\alpha$  excess can be readily identified, but the nature of the stars located on the main sequence just below the turn-off is still unclear. The rather bright detection limit for the emission stars is due to the low sensitivity of the  $H\alpha$  filter.

TABLE 2

CANDIDATE YSOS FOUND WITH *Spitzer* IN THE AREA CENTERED ON NGC 346 OBSERVED WITH ACS. ID NUMBERS SHOWN IN COLUMN 1 ARE FROM BOLATTO ET AL. 2007. CELESTIAL COORDINATES ARE GIVEN IN J2000. MAGNITUDES IN ALL FOUR IRAC CHANNELS ( $3.6\ \mu\text{m}$   $4.5\ \mu\text{m}$   $5.8\ \mu\text{m}$   $8.0\ \mu\text{m}$ ) AND THE  $24\ \mu\text{m}$  CHANNEL OF MIPS ARE GIVEN IN COLUMNS 4, 5, 6, 7 AND 8 RESPECTIVELY. NONE OF THESE OBJECTS WAS DETECTED IN THE LONGER WAVEBANDS OF MIPS ( $70\ \mu\text{m}$  AND  $160\ \mu\text{m}$ ). THE NUMBERS OF THE STARS FOUND TO COINCIDE FROM OUR ACS PHOTOMETRY (PAPER I) WITH THE LOCI OF THESE YSOS (WITHIN  $1''5$ ) AND THE  $F555W$  AND  $F814W$  ( $V$ ,  $I$ ) VEGA MAGNITUDES OF THE BRIGHTEST ONES ARE GIVEN IN THE LAST THREE COLUMNS.

ID	RA (deg)	DEC (deg)	[3.6]	[4.5]	[5.8]	[8.0]	[24]	No	$m_{F555W}$	$m_{F814W}$
185	14.7150	-72.1710	-	14.91	12.62	10.33	-	4	22.55	22.04
186	14.7167	-72.1673	-	14.56	12.58	11.21	-	5	18.39	17.41
187	14.7190	-72.1602	15.17	15.86	12.11	10.31	-	7	23.14	22.50
188	14.7202	-72.1783	15.75	14.97	12.33	10.64	-	4	23.82	21.64
189	14.7231	-72.1624	14.57	15.32	12.52	10.97	-	1	18.86	17.76
190	14.7275	-72.1642	14.57	15.28	12.16	10.55	-	8	20.04	19.46
191	14.7514	-72.1681	-	12.02	10.64	9.19	5.43	6	16.27	15.96
192	14.7582	-72.1762	14.76	14.35	12.59	11.25	-	13	18.99	19.13
194	14.7605	-72.1687	12.38	11.48	10.43	9.22	4.41	10	18.67	17.68
195	14.7622	-72.1765	13.43	13.26	11.49	10.02	-	5	14.45	14.70
196	14.7631	-72.1774	13.93	13.73	11.78	10.24	-	9	18.39	18.26
197	14.7672	-72.1797	-	12.74	11.67	10.31	-	8	16.41	15.11
198	14.7973	-72.1670	-	13.91	11.90	10.02	-	7	15.91	16.09
200	14.8008	-72.1663	11.78	11.28	9.96	8.43	5.10	2	16.77	16.04
203	14.8208	-72.1544	13.90	13.58	11.87	10.12	-	19	19.95	19.51
204	14.8293	-72.1585	-	14.83	12.67	11.12	-	9	19.39	18.41

More recently, Simon et al. (2007) used the data of the S<sup>3</sup>MC survey and detected a significant population of bright, red infrared sources. They expanded the catalog of candidate YSOs in the general area of N 66, and carried out spectral energy distribution (SED) fits based on models by Whitney et al. (2003a,b, 2004) to select  $\approx 110$  YSOs and YSO candidates. Of these, 65 fall within the field of NGC 346 observed with HST/ACS. The positions of these candidate YSOs, kindly provided by J.D. Simon, are overplotted on the isodensity contour map of the PMS stars in the region of NGC 346 in

Fig. 2 (right). The majority of the candidate YSOs from the Simon et al. catalog are located where we find the highest densities of PMS stars. Specifically, almost all of the “definite” YSOs (solid circle symbols) coincide with the density peaks of the map of Fig. 2 (right), and most of them are located in the association and its surrounding area. In addition, four of the PMS clusters we identified earlier (§4) coincide with “definite” YSOs (clusters 2, 3, 4, and 5). According to Simon et al. (2007) the spatial distribution of the YSOs reveal that star formation in N 66 did not proceed from the southwest to-

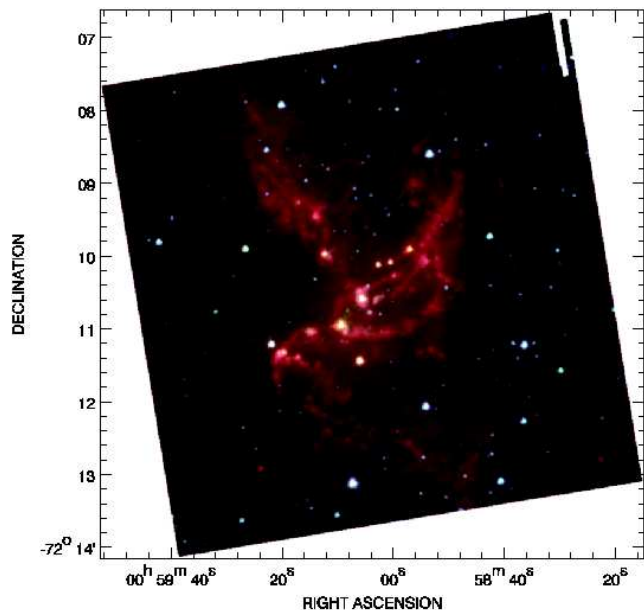


FIG. 13.— Color-composite image of NGC 346/N 66 from *Spitzer*/IRAC with  $3.6\ \mu\text{m}$  shown in blue,  $4.5\ \mu\text{m}$  in green, and  $8\ \mu\text{m}$  in red.

ward the center of the H II region as proposed by Massey et al. (1989). Simon et al. also note that the most-embedded YSOs are more centrally concentrated than the more evolved ones, and that the YSOs are mass segregated with the most massive ones being located closer to the center of N 66. Also, the clumps of molecular gas found by Rubio et al. (2000) from CO(2-1) emission, and the peaks of dust emission at  $7\ \mu\text{m}$  analyzed by Contursi et al. (2000) coincide with many of these YSOs.

## 7. SUMMARY

In this paper we present the results from our photometric study on the recent star formation history of N 66 the brightest H II region in the SMC, related to the OB association NGC 346, as it is recorded in the observed PMS population of the region. Our deep photometry revealed an extremely large number of low-mass PMS stars in the association and the surrounding region, easily distinguishable in the  $V-I$ ,  $V$  CMD. We show that factors such as reddening, binarity and variability can cause a broadening of the positions of these stars in the CMD of the association, wide enough so that they can be misinterpreted as the result of multi-epoch star formation, and not as the product of a single star formation event. We found that a modest reddening like the one we found for the general area of NGC 346 ( $E(B-V) \simeq 0.08$  mag) can make the PMS stars appear younger than what they actually are, and therefore an age of 10 Myr better fits the observed sequence of PMS stars. However, our results do not exclude the possibility of multi-epoch star formation in the area of the association if the reddening is even lower, as suggested from the OB stars of this region ( $E(B-V) \simeq 0.04$  mag). In this case, two star formation events 10 and 5 Myr ago can explain the observed broadening

of the PMS stars due to age spread and factors such as reddening and binarity. No specific dependence of the estimated ages of the PMS stars to their loci within the association, as a signature of sequential star formation, was found.

It has been previously suggested that three different generations of stars occurred through sequential star formation in the region of NGC 346/N 66 (Rubio et al. 2000) within the last 3 Myr (based on the age of the youngest OB stars) and that the PMS stars of NGC 346 represent a star formation event that took place 3 - 5 Myr ago (Nota et al. 2006). However, the study by Massey et al. (1989) based on the presence of evolved  $15\ M_{\odot}$  stars suggests that there might have been earlier star formation events in the region making NGC 346 as old as  $\sim 12$  Myr. In addition, there are recent indications that NGC 346 might host classical Be-type stars (Evans et al. 2006), and if so, the age of the association should be at least 10 Myr, a threshold given by Fabregat & Torrejón (2000) for classical Be-type stars to form. These results fit very well to the hypothesis that star formation in NGC 346 did already occur about 10 Myr ago, as our observations and simulations of the PMS stars suggest.

From star counts based on our ACS photometry we identify at least five PMS clusters across the region, covering a range of ages. On spatial scales from  $0.8''$  to  $8''$  (0.24 to 2.4 pc at the distance of the SMC) the clustering of the PMS stars as computed by a two-point angular correlation function is self-similar with a power law slope  $\gamma \approx -0.3$ . The clustering properties are quite similar to Milky Way star-forming regions like the Orion OB association or  $\rho$  Oph. Thus molecular cloud fragmentation in the SMC seems to proceed on the same spatial scales as in the Milky Way. This is remarkable given the differences in metallicity and hence dust content between SMC and Milky Way star-forming regions.

The youngest PMS stars are located mostly to the north of the bar of N 66, where three PMS clusters are identified. This area is also characterized by a high concentration of candidate YSOs (Simon et al. 2007),  $H\alpha$ -excess stars (found with our photometry), and IR-emission peaks (Rubio et al. 2000). This indicates that star formation probably still takes place in an arc-like feature, as it is outlined by the spatial distribution of these sources. In an accompanying letter, we combine these results with previous multi-wavelength studies of the region to investigate the star formation history, which helped to shape NGC 346/N 66 (Gouliermis et al. 2007b).

D. A. Gouliermis kindly acknowledges the support of the German Research Foundation (Deutsche Forschungsgemeinschaft - DFG) through the individual grant GO 1659/1-1. This paper is based on observations made with the NASA/ESA Hubble Space Telescope, obtained from the data archive at the Space Telescope Science Institute. STScI is operated by the Association of Universities for Research in Astronomy, Inc. under NASA contract NAS 5-26555. It is also based on observations made with the Spitzer Space Telescope, which is operated by the Jet Propulsion Laboratory, California Institute of Technology under a contract with NASA.

## REFERENCES

- Blaauw, A. 1983, *IrAJ*, 16, 141
- Briceño, C., et al. 2001, *Sci*, 291, 93
- Briceño, C., et al. 2005, *AJ*, 129, 907
- Briceño, C., et al. 2007, in "Protostars and Planets V", Eds. B. Reipurth, D. Jewitt, and K. Keil, University of Arizona Press, Tucson, p. 345
- Bolatto, A., et al. 2007, *ApJ*, 655, 212
- Chu, Y.-H. 1997, *AJ*, 113, 1815
- Chu, Y.-H., & Kennicutt, R. C., Jr. 1988, *AJ*, 95, 1111
- Contursi, A., et al. 2000, *A&A*, 362, 310
- Danforth, C. W., Sankrit, R., Blair, W. P., Howk, J. C., & Chu, Y.-H. 2003, *ApJ*, 586, 1179
- Davies, R. D., Elliott, K. H., & Meaburn, J. 1976, *MmRAS*, 81, 89



- de Bruijne, J. H. J., Hoogerwerf, R., & de Zeeuw, P. T. 2001, *A&A*, 367, 111
- Dolphin, A. E. 2000, *PASP*, 112, 1383
- Duquennoy, A., & Mayor, M. 1991, *A&A*, 248, 485
- Efremov, Y. N., & Elmegreen, B. G. 1998, *MNRAS*, 299, 588
- Elmegreen, B. G. 1998, *PASA*, 15, 74
- Elmegreen, B. G. 2006, in “Globular Clusters, Guide to Galaxies” ed. T. Richtler, et al., ESO/Springer (arXiv:astro-ph/0605519)
- Evans, C. J., Lennon, D. J., Smartt, S. J., & Trundle, C. 2006, *A&A*, 456, 623
- Elson, R. A. W., Sigurdsson, S., Davies, M., Hurley, J., & Gilmore, G. 1998, *MNRAS*, 300, 857
- Fabregat, J., & Torrejón, J. M. 2000, *A&A*, 357, 451
- Fukuda N. & Hanawa T. 2000, *ApJ*, 533, 911
- Girardi, L., et al. 2002, *A&A*, 391, 195
- Gomez, M., Hartmann, L., Kenyon, S. J., & Hewett, R. 1993, *AJ*, 105, 1927
- Goodwin, S. P., Kroupa, P., Goodman, A., Burkert, A. 2007, in “Protostars and Planets V”, Eds. B. Reipurth, D. Jewitt, and K. Keil, University of Arizona Press, Tucson, p. 951
- Gouliermis, D., Brandner, W., & Henning, T. 2006a, *ApJL*, 636, L133
- Gouliermis, D. A., Dolphin, A. E., Brandner, W., & Henning, T. 2006b, *ApJS*, 166, 549 (Paper I)
- Gouliermis, D., Brandner, W., & Henning, T. 2005, *ApJ*, 623, 846
- Gouliermis, D. A., Quanz, S. P., & Henning, T. 2007, *ApJ*, 665, 306
- Gouliermis, D., et al. 2007b, submitted to *ApJL*
- Grebel, E. K., Richtler, T., & de Boer, K. S. 1992, *A&A*, 254, L5
- Haberl, F., & Sasaki, M. 2000, *A&A*, 359, 573
- Henize, K. G. 1956, *ApJS*, 2, 315
- Herbst, W., Herbst, D. K., Grossmann, E. J., Weinstein, D. 1994, *AJ*, 108, 1906
- Johnson, H. L., Morgan, W. W. 1953, *ApJ*, 117, 313
- Keller, S. C., Wood, P. R., & Bessell, M. S. 1999, *A&AS*, 134, 489
- Köhler, R., Petr-Gotzens, M. G., McCaughrean, M. J., Bouvier, J., Duchêne, G., Quirrenbach, A., & Zinnecker, H. 2006, *A&A*, 458, 461
- Kontizas, E., Kontizas, M., Gouliermis, D., Dapergolas, A., Korakitis, R., Morgan, D. H. 1999, *IAUS*, 190, 410
- Larson, R. B. 1995, *MNRAS*, 272, 213
- Massey, P., Parker, J. W., Garmany, C. D. 1989, *AJ*, 98, 1305
- Mathieu, R. D. 1994, *ARA&A*, 32, 465
- Nakajima, Y., et al. 1998, *ApJ*, 497, 721
- Nazé, Y., et al. 2002, *ApJ*, 580, 225
- Niemela, V. S., Marraco, H. G., & Cabanne, M. L. 1986, *PASP*, 98, 1133
- Nota, A., et al. 2006, *ApJ*, 640, L29
- Palla, F., & Stahler, S. W. 1999, *ApJ*, 525, 772
- Palla, F., & Stahler, S. W. 2000, *ApJ*, 540, 255
- Petr, M. G., Coude Du Foresto, V., Beckwith, S. V. W., Richichi, A., & McCaughrean, M. J. 1998, *ApJ*, 500, 825
- Pollock, A. M. T. 2002, in ASP Conf. Ser., 260, Interacting Winds from Massive Stars, ed. A. F. J. Moffat & N. St Louis (San Francisco: ASP), 363
- Preibisch, T., & Zinnecker, H., 1999, *AJ*, 117, 2381
- Prosser, C. F., Stauffer, J. R., Hartmann, L., Soderblom, D. R., Jones, B. F., Werner, M. W., & McCaughrean, M. J. 1994, *ApJ*, 421, 517
- Pudritz, R. E. 2002, *Science*, 295, 68
- Relaño, M., Peimbert, M., & Beckmann, J. 2002, *ApJ*, 564, 704
- Rochau, B., Gouliermis, D. A., Brandner, W., Dolphin, A. E., & Henning, T. 2007, *ApJ*, 664, 322
- Rubio, M., Contursi, A., Lequeux, J., Probst, R., Barb  , R., Boulanger, F., Cesarsky, D., Maoli, R. 2000, *A&A*, 359, 1139
- Sabbi, E., et al. 2007, *AJ*, 133, 44
- Sanduleak, N. 1968, *AJ*, 73, 34
- Scalo, J. M. 1985 in *Protostars and Planets II*, University of Arizona Press, 201
- Sherry, W. H. 2003, Ph.D. Thesis, State University of New York at Stony Brook
- Sherry, W. H., Walter, F. M., Wolk, S. J. 2004 *AJ*, 128, 2316
- Shu, F. H., Adams, F. C., & Lizano, S. 1987, *ARA&A*, 25, 23
- Siess, L., Dufour, E., & Forestini, M. 2000, *A&A*, 358, 593
- Simon, J. D., et al. 2007, accepted for publication in *ApJ* (arXiv:astro-ph/0707.3998)
- Stahler, S. W., & Palla, F. 2005, *The Formation of Stars*, ISBN 3-527-40559-3, Wiley-VCH
- Tout, C. A. 1991, *MNRAS*, 250, 701
- Vanhala, H. A. T., & Cameron, A. G. W. 1998, *ApJ*, 508, 291
- V  zquez-Semadeni, E. 2004, *Ap&SS*, 292, 187
- Vel  zquez, P. F., Koenigsberger, G., & Raga, A. C. 2003, *ApJ*, 584, 284
- Walborn, N. R., et al. 2000, *PASP*, 112, 1243
- Walborn, N. R. 1978, *ApJ*, 224, L133
- Walborn, N. R., & Blades, J. C. 1986, *ApJ*, 304, L17
- Wessolowski, U. 1996, in *MPE Rep. 263, R  ntgenstrahlung from the Universe*, ed. H. U. Zimmerman, J. E. Tr  mper, & H. Yorke, 75
- Whitney, B. A., Wood, K., Bjorkman, J. E., & Wolff, M. J. 2003, *ApJ*, 591, 1049
- Whitney, B. A., Wood, K., Bjorkman, J. E., & Cohen, M. 2003, *ApJ*, 598, 1079
- Whitney, B. A., Indebetouw, R., Bjorkman, J. E., & Wood, K. 2004, *ApJ*, 617, 1177
- Woitas, J., Leinert, C., K  hler, R. 2001, *A&A*, 376, 982
- Ye, T., Turtle, A. J., & Kennicutt, R. C., Jr. 1991, *MNRAS*, 249, 722